DESIGN OF A 5^{th} HARMONIC GENERATOR FOR A Nd^{+}:YAG LASER SOURCE FOR OPTICAL LITHOGRAPHY

by

Lisa Leinbaugh

Memorandum No. UCB/ERL M92/144

16 December 1992

DESIGN OF A 5^{th} HARMONIC GENERATOR FOR A Nd^{+}:YAG LASER SOURCE FOR OPTICAL LITHOGRAPHY

by

Lisa Leinbaugh

Memorandum No. UCB/ERL M92/144

16 December 1992

ELECTRONICS RESEARCH LABORATORY

College of Engineering
University of California, Berkeley
94720

DESIGN OF A 5^{th} HARMONIC GENERATOR FOR A Nd^{+}:YAG LASER SOURCE FOR OPTICAL LITHOGRAPHY

by

Lisa Leinbaugh

Memorandum No. UCB/ERL M92/144

16 December 1992

ELECTRONICS RESEARCH LABORATORY

College of Engineering
University of California, Berkeley
94720

Design of a 5^{th} Harmonic Generator for a Nd^+:YAG Laser Source for Optical Lithography

Lisa Leinbaugh
M.S. Project
Professor Oldham
University of California, Berkeley

December 16, 1992

Abstract

The design of a harmonic generator for use in conjunction with a Nd^+:YAG laser, in a novel deep-UV optical lithography source, is discussed in detail. The design strategy used for this application can be generalized and applied to the design methodology of any multi-stage nonlinear optical system. The main issues addressed are nonlinear materials and parameters, conversion efficiencies, power balancing, polarization constraints, and heat flow management.

1 Introduction

The quest for ever smaller feature sizes in semiconductor circuits leads to the desire for ever shorter wavelengths in patterning. Optical lithography continues to be the least expensive method for patterning wafers and several generations of optical lithography remain to be developed in pursuit of these smaller wavelengths. The standard ultraviolet wavelength used today in industry is the I-line of a mercury arc lamp with a wavelength of 365nm. The next generation deep-UV wavelength under development is 248nm produced by the KrFl eximer laser. This system can deliver minimum linewidths of around 0.35 microns. 213nm is proposed as a succeeding and perhaps final generation of optical lithographic wavelengths. The minimum linewidth obtained using 213nm is expected to be approximately 0.18 microns.

The 213nm lithography source consists of a solid state Nd^+:YAG laser with a wavelength of 1064nm followed by nonlinear frequency conversion optics which quintuple the frequency, producing 213nm radiation. This laser source has several advantages. Unlike the eximer lasers, the Nd^+:YAG laser can be seeded providing a very narrow frequency bandwidth on the order of 0.1 pm. This narrow bandwidth is also essential for allowing the use of refractive optics. The narrow bandwidth is required because the imaging optics cannot be chromatically corrected since there is only one refractive optical material available at this deep-UV wavelength. The Nd^+:YAG laser is also advantageous because it is a solid state laser and thus it is low maintenance and avoids the hazards associated with toxic gases. The ND+:YAG laser system will also have a comparably small footprint, an important consideration in the expensive clean room environment. Another reason 213nm is an attractive wavelength is that the IR absorption edge of fused silica, the only presently available deep-UV material for imaging optics, begins around 200nm. Even a small absorption is detrimental to the image quality given the large thickness of fused silica used and the sensitivity of the alignment in the patterning. At the 213nm wavelength the refractive imaging optics are still feasible, while the shorter frequency is a significant advance in achieving smaller patterns.

The first generation 213nm system was constructed by [Partlo 92] and is a 0.25 Watt, flashlamp-pumped, 10 Hz, Nd^+:YAG laser followed by a fifth harmonic generator. The harmonic generator consists of three nonlinear crystals. The first is a type II KD*P doubling crystal producing the second harmonic. The second stage is a type II KD*P crystal cut for generating the third harmonic. A waveplate is needed between the second and third stages to correct the polarizations of the second and third harmonics with respect to each other. The final crystal is a type I BBO mixing crystal which mixes the second and the third harmonics to produce the fifth

Parameter	Old System	New System Before SBS	After SBS
Repitition Rate [Hz]	10	1000	1000
Average Power [Watts]	4.1	50	35
Pulse Energy [J]	0.41	0.05	0.035
Pulse Duration [ns]	8	5	~ 1.0
Beam Diameter [mm]	6	3-5	3-5
Peak Pulse Power [MW/cm^2]	180	50	~ 200

Table 1: A comparison of the first and second generation systems, including the effects of the SBS pulse compression optics.

---

harmonic. With this system the patterning of 0.2 micron lines and spaces has been demonstrated. The new laser system will be a diode-pumped, seeded, Q-switched, Nd^+:YAG laser with SBS (Stimulated Brillouin Scattering) pulse compression optics, followed by the harmonic generator. The new laser will have a repetition rate of 1000 Hz, with 50 Watts in the infrared, which after pulse compression will decrease to around 35 Watts. The pulse width will be shortened from 5ns to approximately 1 ns using the SBS compression optics. The pulse compression is necessary to increase the peak pulse power for efficient harmonic conversion in the harmonic generator. The output power in the fifth harmonic (213nm) should be on the order of a few Watts. Table 1 compares the parameters of the first and second generation lasers.

The design of the harmonic generator is the topic of this report. There are several motivations for a redesign of the nonlinear optics. The first and foremost is the desire for better management of heat flow. The current system already reveals problems associated with heating in the BBO crystal. The new system will have a higher average power and thus the heating is expected to be much more critical. The new system will also be designed to take the power balancing between the various stages into consideration. Finally, new materials will be considered. The primary goal of the harmonic generator is to achieve the highest possible efficiency in converting the fundamental into the fifth harmonic. In the new system the goal is to maintain or improve the conversion efficiency even with increased average power and the same peak pulse power.

The first section will give an overview of the basic ideas on harmonic generation. Next several nonlinear materials will be discussed and the nonlinear parameters of the appropriate materials are calculated. Using the parameters calculated in section three, section four goes on to calculate the conversion efficiencies of the materials and

nonlinear interactions of interest. The whole system is then considered and balance of power between the different harmonics is examined in section five. At this point several designs are proposed and polarizations are considered. The final section deals with the heating problems and the design of a prism beam compressor to deal with the problem.

2 Background

Nonlinear optical phenomena were first discovered and utilized with the advent of the laser. The laser was a necessary precursor since nonlinear phenomena are only observable at the high intensities unique to the laser. In the everyday world only the linear interactions of light and matter are observed. These interactions can be simply modeled as follows. Light can be viewed as an oscillating electric field, and matter as a collection of electric dipoles. When a material is subjected to an oscillating electric field of normal intensity, the dipoles in the material will oscillate in response to the applied field at the frequency of the field. The dipoles will then radiate a field at the frequency of oscillation. This description accounts for the linear optical phenomena, such as transmission of light through glass, with which we are familiar.

For high intensity fields the situation is more complex. The dipoles, in addition to oscillating at the fundamental frequency, will also oscillate at harmonics of the fundamental frequency. The following equation shows the polarization response P as a function of the electric field E, where χ is the susceptibility of the medium:

$$P = \varepsilon_0(\chi^{(1)}E + \chi^{(2)}E^2 + \chi^{(3)}E^3 + \cdots +). \tag{1}$$

Generally the first term is a sufficient approximation for describing what occurs under normal illumination. At high intensity, however, the higher orders become important. In particular the harmonic generation phenomena are due to the squared term of the electric field. In the case of second harmonic generation one input frequency ω is used and the dipole will oscillate at twice the fundamental frequency 2ω thus generating the second harmonic. In frequency mixing there will be two input frequencies ω_1 and ω_2, which beat together causing the dipole to oscillate and thus radiate at the sum frequency $\omega_3 = \omega_1 + \omega_2$. [Butcher 90, § 1]

Another way of looking at nonlinear interactions is the quantum mechanical photon picture. From this viewpoint frequency doubling consists of two photons in the material combining to produce one photon at twice the frequency. Since the energy of each photon is $\hbar\omega$, the frequency of the created photon must be 2ω according to the consevation of energy principle. For the frequency mixing case, one photon at

frequency ω_1, and one photon at frequency ω_2 are annihlated and replaced by one photon at frequency ω_3. Again by the conservation of energy principle the sum frequency generation relation is $\omega_3 = \omega_1 + \omega_2$. This picture illustrates the same result as the dipole model. [Yariv 89, §17.6]

For an efficient transfer of power into a higher harmonic during frequency generation, the different frequency waves must travel in phase. However, the nonlinear crystal is a dispersive medium (the index of refraction is dependent on frequency). There will be destructive interference between the waves because they travel at different velocities and become out of phase (phase mismatched). The phase mismatch will limit the conversion efficiency. A technique known as phase matching is used to correct for these normal dispersion effects in the nonlinear crystal. To accomplish phase matching, a crystal which is highly birefrigent is needed. A birefringent material has two different indices of refraction in orthogonal directions. The ordinary index of refraction n_o is independent of orientation, while the extraordinary index $n_e[\theta]$ is dependent upon the direction of propagation. The crystal is cut in such a way that the different frequency waves will travel at the same velocity and thus remain in phase. The dispersion of the material is compensated for by the angle tuning of the crystal. [Hon 79] Phase matching greatly limits the choice of nonlinear crystals. It is particularly difficult to find a material which is sufficiently birefrigent to compensate for the dispersion at high frequencies. The following section deals with the selection of appropriate nonlinear materials and calculating their nonlinear properties.

3 Evaluation of Nonlinear Materials and Parameters

3.1 Materials

Materials are a very important consideration in the design of nonlinear optics. New materials are continuously being developed. Some of the important requirements for a suitable nonlinear material are a high nonlinearity, high damage threshold, reasonable angular acceptance, no absorption, and the availability of the material in question.

Many popular nonlinear materials were found to have unacceptable damage thresholds for our application, or simply not have a interaction at the required frequencies. The materials under consideration for working with the Nd^+:YAG harmonic frequencies were KDP, KD*P, KTP, BBO and LBO. Additionally two fundamental kinds of

phase matching, critical and noncritical, are considered.

Potassium dihydrogen phosphate (KDP) is one of the first used and still quite common materials for harmonic generation. [Eimeral 87c] Unfortunately KDP has an absorption edge in the IR right around the Nd^+:YAG wavelength, and this absorption precludes its use. This absorption eliminates the use of KDP for any of the interactions since in our simple design the fundamental beam travels through all the crystals in the system. The IR absorption edge can be pushed deeper by deuteration of $> 90\%$. The deuterated form, KD*P is a strong candidate for many of the interactions as it has a fair nonlinear coefficient balanced by a large angular acceptance. KD*P has a damage threshold of between 3 and 5 GW/cm^4 which is well above our projected peak power of .2 GW/cm^2. This material was examined in detail and seems to be the best choice for many of the desired interactions. There is also a temperature tuned interaction doubling the second harmonic which will be discussed in the following section dealing with efficiencies.

Potassium titanyl phosphate (KTP) has a high nonlinear coefficient, and would seem to be the ideal choice for doubling, but unfortunately suffers optical damage at high average powers. In [Tyminski 90] it is shown that at room temperature "dark tracks" appear in the material at average powers of 20W. These "dark tracks" are accompanied by increasing absorption and degrade the conversion efficiency finally destroying the crystal. In the system currently under design we expect to use around 35W of average power and thus we must eliminate this material a a potential candidate. If the crystal is heated to about 170°C the "dark tracks" can be avoided but astigmatism of the intensity profile and degradation of the beam occurs even at 20W. Thus KTP was eliminated from the useful nonlinear materials for this particular application.

Beta barium borate (BBO), a recently introduced negatively uniaxial material, is the only suitable material for the $1 + 4 \rightarrow 5$ or $2 + 3 \rightarrow 5$ mixing interactions of the Nd^+:YAG harmonics. BBO is a very promising material for many of the other interactions as well [Eimeral 87b]. BBO has a high damage threshold of $13.5 \pm 2GW/cm^2$ for a 1 ns pulse at 1064nm and $7.0 \pm 1GW/cm^2$ for a 1ns pulse at 532nm [Chen 86]. While BBO has a high nonlinear coupling it has the drawback of having a small angular acceptance. This material was considered in great detail for use in generating all of the required harmonics.

A final material under consideration is LBO. This material is primarily interesting in the capacity of a noncritically phase matched (NCPM) doubler for generating the second harmonic [Ukachi 90]. As a critically phase matched material, BBO is a better choice both due to a higher nonlinear coefficient and in terms of cost and

availability, but LBO may offer higher conversion efficiencies as a NCPM doubler. In fact what seems to be the limiting factor for LBO is the difficulty in obtaining a high quality material. This material should definitely be kept in mind for future use as the availability of high quality materials should increase and make it a feasible alternative. With this in mind the temperature tuning characteristics are calculated in the chapter dealing with efficiencies.

In summary, for the first doubling stage KD*P, BBO and NCPM LBO will be considered in greater depth. For the second stage the materials of interest are KD*P, BBO and NCPM KD*P. For the final stage which mixes to produce the fifth harmonic, BBO is the only available material. The following section describes in detail the calculation of the relevant nonlinear parameters, and the next chapter describes the conversion efficiency calculations.

3.2 Calculating Nonlinear Parameters

This section delineates the equations for calculating the nonlinear parameters for critically phase matched interactions. The nonlinear parameters are used to calculate the theoretical conversion efficiencies for the various nonlinear reactions and materials shown in the next chapter. These parameters allow a comparison of the different materials and nonlinear interactions independent of the crystal geometry. Using Eimeral's methodology the angular sensitivity of a crystal can be compensated for by focusing and thus adjusting the input intensity. Thus it is important to calculate a "figure of merit" which can be used to compare different crystals. The parameters for the interactions of interest for BBO and KD*P were calculated and tabulated in Table 2 and Table 3. Both BBO and KD*P are negative uniaxial materials, in other words, the extraordinary index of refraction is less than or equal to the ordinary index of refraction, and there is only one optic axis. The noncritically phase matched interactions will be addressed in the chapter on efficiencies.

The phase matching angle is the angle, with respect to the optic axis, at which the incoming light must enter the crystal in order to be properly phase matched [Hon 79]. This angle is derived from the combination of the index ellipsoid equation and the type of phase matching requirement. The phase matching angle depends on the ordinary and extraordinary indices of refraction of the particular material. The following equation gives the phase matching angle for type I phase matching.

$$\theta_m = \arcsin\sqrt{\frac{1/N^2 - 1/n_{o3}^2}{1/n_{e3}^2 - 1/n_{o3}^2}}, \tag{2}$$

where

$$N = \frac{1}{\omega_3}[\omega_1 n_o + \omega_2 n_o]$$

and

$$\omega_3 > \omega_2 \geq \omega_1.$$

For type II phase matching, the equation must be solved iteratively.

$$\left[\frac{\cos^2[\theta_m]}{n_{o3}^2} + \frac{\sin^2[\theta_m]}{n_{e3}^2}\right]^{-1/2} = \frac{1}{\omega_3}\left[\omega_2 n_{o2} + \omega_1\left(\frac{\cos^2[\theta_m]}{n_{o1}^2} + \frac{\sin^2[\theta_m]}{n_{e1}^2}\right)^{-1/2}\right] \tag{3}$$

For type III phase matching the following equation applies.

$$\left[\frac{\cos^2[\theta_m]}{n_{o3}^2} + \frac{\sin^2[\theta_m]}{n_{e3}^2}\right]^{-1/2} = \frac{1}{\omega_3}\left[\omega_1 n_{o1} + \omega_2\left(\frac{\cos^2[\theta_m]}{n_{o2}^2} + \frac{\sin^2[\theta_m]}{n_{e2}^2}\right)^{-1/2}\right] \tag{4}$$

The different "type"s of phase matching refer to the polarization restrictions on the incoming light waves. For type I phase matching, both input waves must be polarized in the n_o direction, and the output wave will be polarized along the n_e direction. In type II phase matching, the lowest frequency wave enters along the n_e axis and the equal or higher frequency wave must enter along the other axis. The wave will again exit along the n_e axis. Type III phase matching is the reverse of type II phase matching. Type III is relatively rare since the crystal must be highly birefringant to accomplish this type of phase matching.

The angular sensitivity is a measure of how large the phase mismatch becomes with deviations from the phase matching angle [Eimeral 87b]. The phase mismatch is the non-zero difference between the propagation vectors of the three waves. The angular sensitivity is derived by writing the phase mismatch relation in terms of the frequency and the indices of refraction. Then the derivative of the phase mismatch is taken with respect to the angle. By remembering that the ordinary index is constant reguardless of direction we can set the derivative of n_o to zero. The relationship for Type I phase matching can be then written as

$$\beta_\theta = \frac{2\pi}{\lambda_3}\left(\frac{\sin[\theta_m]\cos[\theta_m][1/n_{e3}^2 - 1/n_{o3}^2]}{\sqrt[3/2]{\frac{\cos^2[\theta_m]}{n_{o3}^2} + \frac{\sin^2[\theta_m]}{n_{e3}^2}}}\right). \tag{5}$$

The more complex relation describing the angular sensitivity for type II phase matching is

$$\beta_\theta = \frac{2\pi}{\lambda}\sin[\theta]\cos[\theta]\left[\frac{c(1/n_{e3}^2 - 1/n_{o3}^2)}{\sqrt[3/2]{\frac{\cos^2[\theta]}{n_{o3}^2} + \frac{\sin^2[\theta]}{n_{e3}^2}}} - \frac{a(1/n_{e1}^2 - 1/n_{o1}^2)}{\sqrt[3/2]{\frac{\cos^2[\theta]^2}{n_{o1}^2} + \frac{\sin^2[\theta]}{n_{e1}^2}}}\right], \tag{6}$$

where

$$\omega_1 = a\omega_o,\ \omega_2 = b\omega_o,\ \omega_3 = c\omega_o.$$

The type III angular sensitivity relation is the same as the type II equation except b is substituted for a and n_{x2} is substituted for n_{x1}.

The angular bandwidth is defined as the FWHM of the output intensity *vs.* angle, centered on the phase matching angle. [Eimeral 87b]

$$\Delta\Theta = \frac{4A\ell}{\beta_{theta}}, \tag{7}$$

where

$$A = 1.392.$$

The effective nonlinear coupling for a particular nonlinear reaction is described by the nonlinear coefficient for that reaction. The nonlinear coefficients are determined by the crystal structure of the particular material. For BBO [Eimeral 87b] the effective nonlinear coefficient can be calculated for type I interactions using the following equation

$$d_{eff} = d_{31}\sin[\theta] - d_{11}\cos[\theta]\cos[3\phi]. \tag{8}$$

For type II phase matching the relation is

$$d_{eff} = d_{11}\cos[\theta]^2\sin[3\phi] \tag{9}$$

where

$$d_{11} = 1.6 \pm 0.4pm/V,$$

$$|\frac{d_{31}}{d_{11}}| < 0.05,$$

and

$$\phi = 45°.$$

The nonlinear coefficients for KD*P take a different form since the crystal structure of KD*P differs from BBO. The values in the chart for KD*P were taken from the paper by Eimeral on KDP and its isomorphs [Eimeral 87c, p 111].

Frequency	Mixing	Type	Θ_m	β_Θ 1/cm*rad	$\Delta\Theta$ rad 10^{-4}	β_T 1/C cm	ΔT C	d_{eff} pm/V	C $GW^{-\frac{1}{2}}$	P_{th} GW	C^2 GW^{-1}
2w	1+1	I	22.9	10900	5.10	0.11	50.6	1.07	2.66	0.19	7.08
	1+1	II	32.6	7080.3	7.86	0.15	37.1	0.80	2.06	0.13	4.24
3w	1+2	I	31.1	20479.4	2.71	0.36	15.5	1.01	3.72	0.34	13.87
	1+2	II	38.2	15968.4	3.48	0.42	13.3	0.70	2.67	0.40	7.15
	1+2	III	59.7	5398.7	10.3	0.42	13.3	0.29	1.11	0.27	1.23
4w	2+2	I	47.6	32982.8	1.68	1.4	3.98	0.82	3.95	0.79	15.63
	2+2	II	84.7	3138.0	17.7	0.137	40.6	0.01	0.05	45	0.003
	1+3	I	40.3	33747.0	1.65	1.4	3.98	0.91	4.38	0.67	19.14
	1+3	II	46.6	26633.3	2.08	0.21	27	0.53	2.64	1.15	6.96
	1+3	III	None								
5w	1+4	I	51.1	47955.2	1.16	0.34	16.2	0.77	4.48	1.30	20.03
	1+4	II	57.2	37679.3	1.48	0.274	20.3	0.33	1.99	4.07	3.95
	1+4	III	None								
	2+3	I	69.5	29878.9	1.86	0.34	16.2	0.47	2.76	1.33	7.60
	2+3	II	None								
	2+3	III	None								

Table 2: Table of parameters for BBO

The nonlinear coupling parameter, useful in calculating the threshold power and drive is calculated as following

$$C = \frac{c\,2.728\,d_{eff}}{\lambda_o\sqrt{n_1 n_2 n_3}}, \tag{10}$$

where n_x are the appropriate indices of refraction for the particular interaction taking place, and d_{eff} is in pm/V, λ_o is in μm, and C is in GW$^-$1/2.

The threshold power is the minimum power which allows for a reasonable conversion efficiency.

$$P_{th} = \left(\frac{\beta_\theta \lambda_o}{C}\right)^2 \tag{11}$$

The drive is a parameter independent of the crystal geometry which can be used as a "figure of merit" in comparing different materials and interactions is calculated as follows

$$\eta_o = C^2 \ell^2 I. \tag{12}$$

Frequency	Mixing	Type	Θ_m	β_Θ 1/cm*rad	$\Delta\Theta$ rad 10^{-4}	β_T 1/C cm	ΔT C	d_{eff} pm/V	C $GW^{-\frac{1}{2}}$	P_{th} GW	C^2 GW^{-1}
2w	1+1	I	22.9	10900	5.10	0.11	50.6	1.07	2.66	0.19	7.08
	1+1	II	32.6	7080.3	7.86	0.15	37.1	0.80	2.06	0.13	4.24
3w	1+2	I	31.1	20479.4	2.71	0.36	15.5	1.01	3.72	0.34	13.87
	1+2	II	38.2	15968.4	3.48	0.42	13.3	0.70	2.67	0.40	7.15
	1+2	III	59.7	5398.7	10.3	0.42	13.3	0.29	1.11	0.27	1.23

Table 3: Table of parameters for KDP

A final property of nonlinear interaction to be considered is the walk-off. Walk-off occurs when the phase-matching is accomplished at at an angle off the optic axis. In this situation there is a small angle between the power flow in the first harmonic and the power flow in the second harmonic. This walk-off will cause the volume, over which further harmonic generation can occur, to decrease as the two beams separate. The formula describing this situation is as follows

$$\rho = \arctan^{-1}[\frac{n_{o1}^2}{2}(\frac{1}{n_{e2}^2} - \frac{1}{n_{o2}^2})]\sin[2\theta_m]. \tag{13}$$

where ρ is the walk-off angle. While in some cases this parameter may be critical, in the case for BBO and KD*P the angular sensitivity are much greater problems that the walk-off.

4 Calculating Crystal Efficiencies

One of the most important criteria for choosing a particular crystal or interaction is the conversion efficiency. The conversion efficiency is simply the amount of harmonic power generated compared to the amount of input power. There are several commonly used methods for calculating the conversion efficiencies.

One method of calculating the conversion efficiency is described in [Eimeral 87b]. This method is only valid for low efficiency crystals because depletion is not taken into account. The dephasing is taken into account by including the unavoidable phase

mismatch term Δk. The equation for the maximum conversion efficiency η_{max} is

$$\eta_{max} = \eta_o \frac{\sin^2[\frac{1}{2}\Delta kl]}{(\frac{1}{2}\Delta kl)^2}, \tag{14}$$

where η_o is the drive (described in the previous section), l is the crystal length, and Δk is the phase mismatch due to the natural divergence of the beam. This simple formula is only valid for crystals with a drive less than 1 ($\eta_o < 1$). For higher efficiencies the depletion of power in the crystal must be taken into account or else the results are severely over optimistic.

A more rigorous method used for high power systems ($\eta_o > 1$), can be found in [Eimeral 87a]. This approximation takes into account the depletion of the pump power but not the dephasing, i.e. this approximation assumes Δk is zero.

$$\eta_{max} = \tanh^2 \sqrt{\eta_o} \tag{15}$$

where again η_o is the drive.

The exact solution must be used in the high efficiency case where both dephasing and depletion are important. The exact solution also yields an optimum length for the crystal which the approximations do not [Eimeral 87a]. The exact solution is

$$\eta_{max} = \tanh^2[\frac{1}{2}\tanh^{-1}(sn[2\eta_o^{1/2}, 1 + \frac{\delta^2}{4\eta_o}])] \tag{16}$$

Where sn is a Jacobi elliptic function, η_o is the drive and

$$\delta = \frac{1}{2}\Delta kl. \tag{17}$$

Figure 1 compares the different methods for calculating efficiencies.

Because of the high power, the exact Jacobian solution was applied to find accurate conversion efficiencies of all the interactions under consideration. For the efficiency calculations the intensity was assumed to be 180 MW/cm^2, the pulse diameter was assumed to be 0.6 cm, and all other values were taken from the parameter tables in chapter three. Figure 2 compares the maximum conversion efficiencies versus crystal lengths for all interactions of interest for the first stage doubling crystal. Figure 3 compares the maximum conversion efficiencies versus crystal lengths for all the interactions for the second stage in either quintupling scheme. Figure 4 compares the maximum conversion efficiencies vs. lengths for the possible, stage three, fifth harmonic crystals. Table 4 tabulates, for each stage, the different interaction possibilities and their maximum conversion efficiencies and corresponding crystal lengths. Using

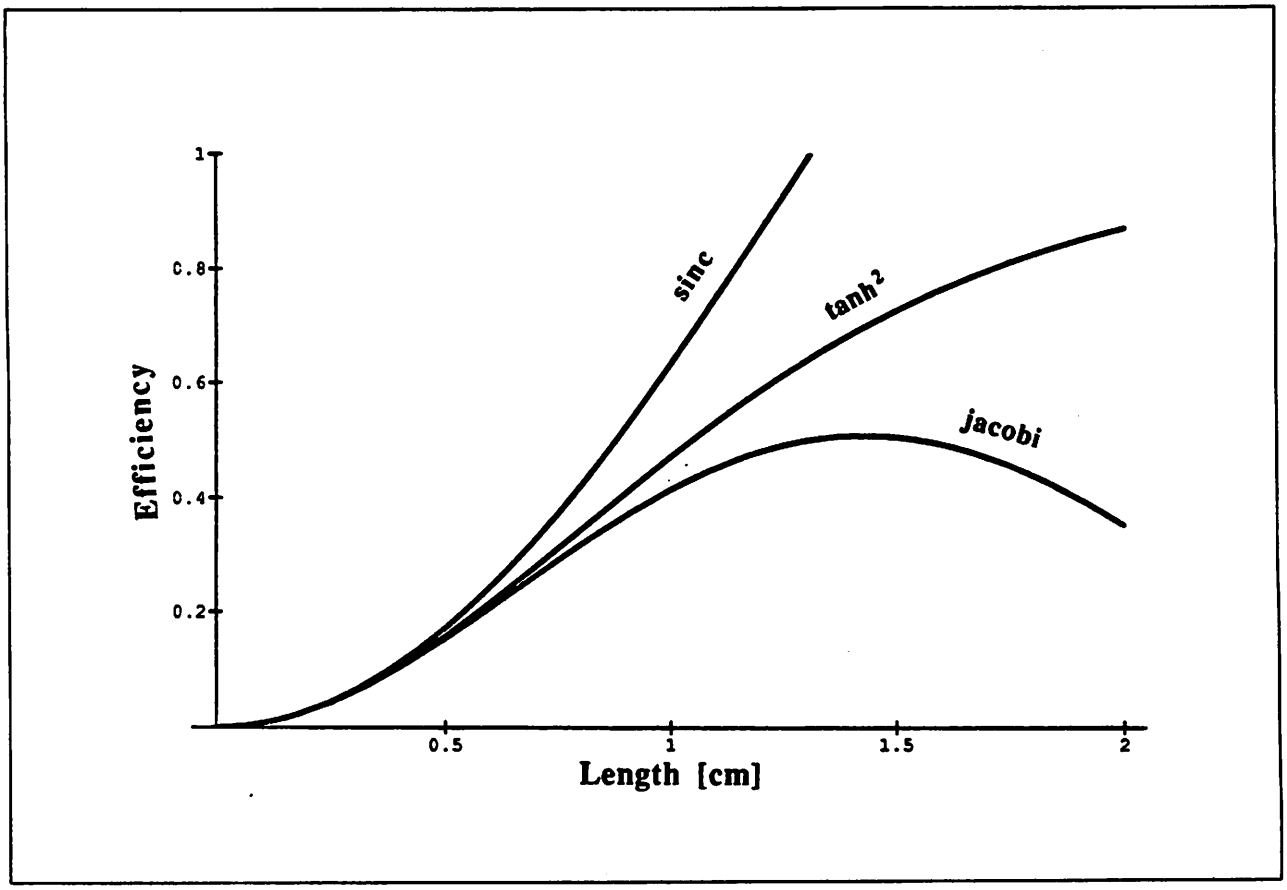

Figure 1: Three methods for calculating efficiencies.

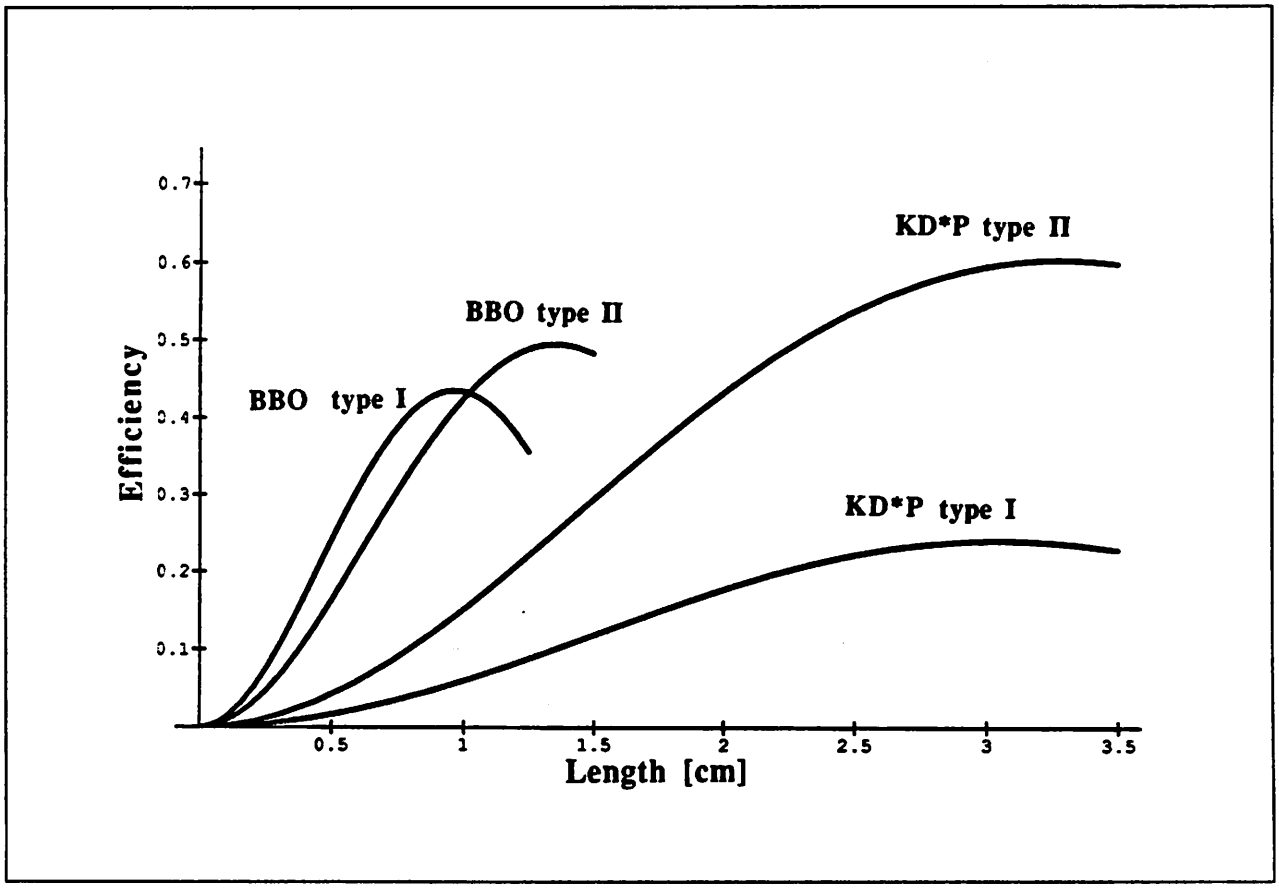

Figure 2: Efficiencies for the first stage doubling crystal.

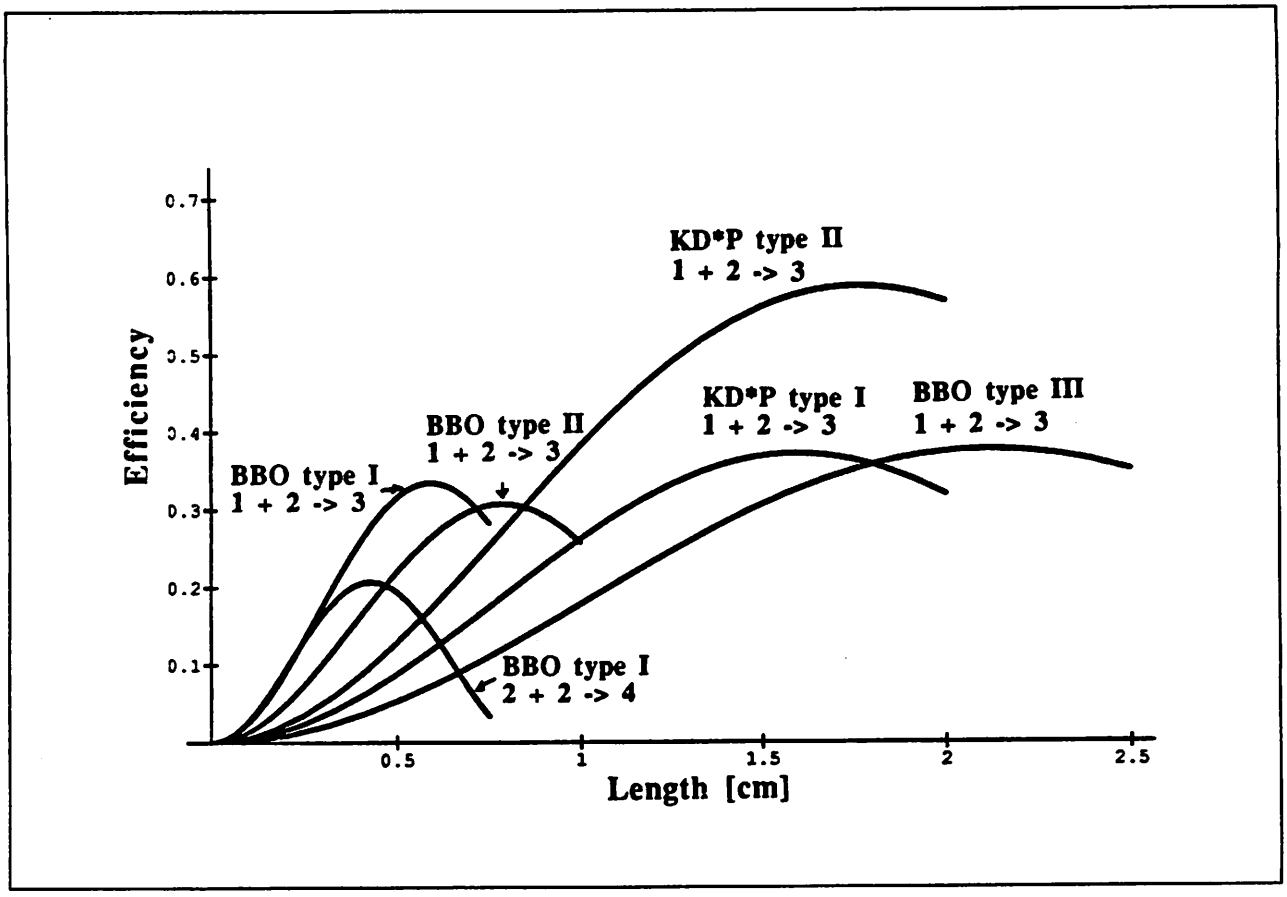

Figure 3: Efficiencies for the second stage crystals.

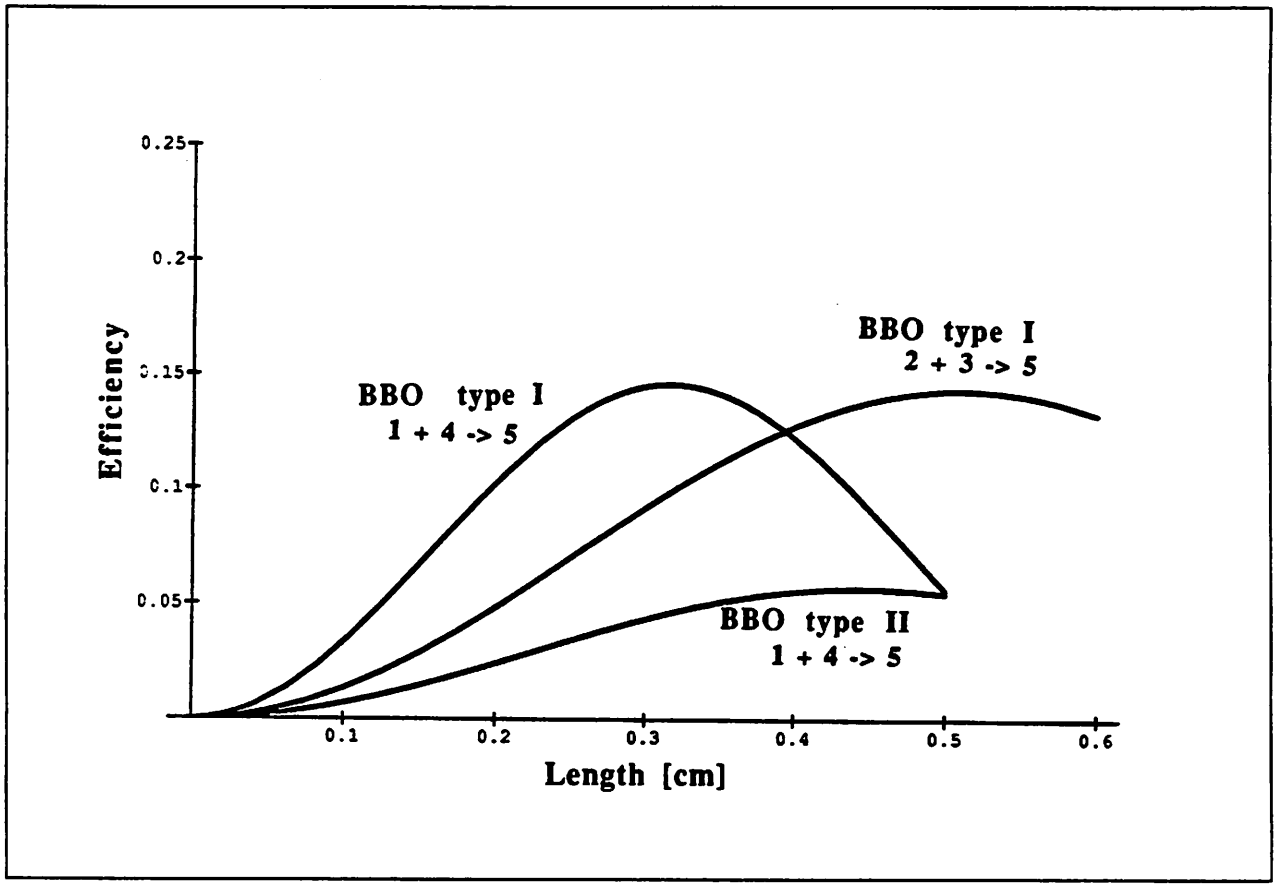

Figure 4: Efficiencies for the third stage fifth harmonic crystals.

Stage 1

Crystal	Mixing	Type	Length [cm]	η_{max} [%]
BBO	1 + 1	I	0.97	43.5
BBO	1 + 1	II	1.35	49.5
KD*P	1 + 1	I	3.1	24
KD*P	1 + 1	II	3.3	60

Stage 2

Crystal	Mixing	Type	Length [cm]	η_{max} [%]
BBO	2 + 2	I	0.43	21
BBO	1 + 2	I	0.60	33.4
BBO	1 + 2	II	0.78	31
BBO	1 + 2	III	2.10	38
KD*P	1 + 2	I	1.7	37
KD*P	1 + 2	II	1.8	58

Stage 3

Crystal	Mixing	Type	Length [cm]	η_{max} [%
BBO	1 + 4	I	0.32	15
BBO	1 + 4	II	0.45	6
BBO	2 + 3	I	0.5	14.3

Table 4: Maximum efficiencies and corresponding crystal lengths.

these figures, the maximum attainable efficiencies of each critically phase-matched crystal, and the length required to attain this length, can easily be compared.

The conversion efficiencies for two noncritically phase matched (NCPM) crystals were also calculated. In the case of NCPM crystals, the phase matching angle θ_m is 90°, such that the indices of refraction are n_o in both directions and the angular sensitivity is eliminated. Dephasing is caused by temperature sensitivity as opposed to angular sensitivity. The noncritically phase-matched crystal is tuned by heating it to a specific temperature instead of a very precise angle [Hon 79]. The two noncritically phase-matched crystals which are applicable to the two quintupling schemes under consideration are LBO for the first stage doubling in either scheme, and KD*P for doubling the second harmonic to create the fourth harmonic. The efficiencies were calculated using the exact Jacobian equation where the angular sensitivity was replaced by the temperature sensitivity.

The noncritically phase matched LBO crystal has type I phase-matching at a temperature of 140°C. The temperature sensitivity value for LBO was calculated to be 14.69 $C^{-1}cm^{-1}$ from a temperature bandwidth reported in [Ukachi 90], the d_{eff} value used was 0.765 pm/V, and from these values a c parameter of 1.94 $GW^{-1/2}$ was calculated. The index of refraction used was 1.6 . The curves in Figure 5 show the result for several ΔT values as these depend on absorption in the material and at this time we have no hard data to determine what that value will be. One problem particular to LBO is that the material is biaxial and the expansion coefficients are quite different along the different axes. This causes mechanical difficulties with applied anti-reflection coatings.

The NCPM KD*P crystal used for doubling the second harmonic to produce the fourth harmonic has type I phase matching at 40.6°C. A temperature sensitivity value of 0.149 $C^{-1}cm^{-1}$ was calculated from a temperature bandwidth value of 6.7 C-cm in [Hon 79]. The values of d_{eff} = .367 pm/V and c = 2.02 $GW^{-1/2}$ were taken from [Eimeral 87c]. The indices of refraction were also obtained from [Eimeral 87c]. Figure 6 shows the efficiency versus length curves for several values of ΔT across the crystal face. The concern with using a noncritically phase-matched crystal in the new high power system is that the temperature differential across the crystal face will be too high for good phase matching. This problem may, in large part be reduced by the slab geometry idea discussed in section seven, but should be examined with care before committing to using one of these crystals.

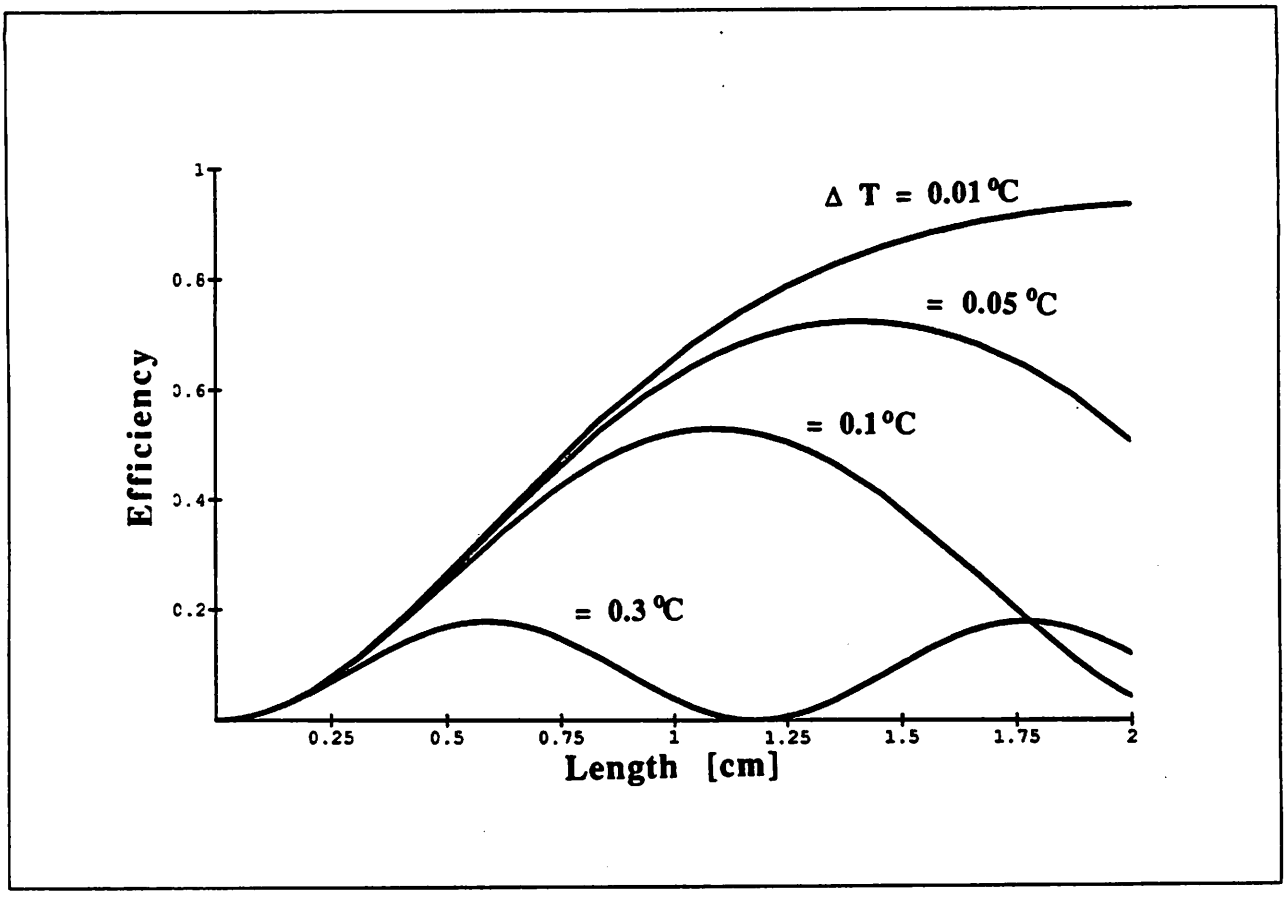

Figure 5: Efficiency curves for a NCPM LBO doubler with different temperature differentials.

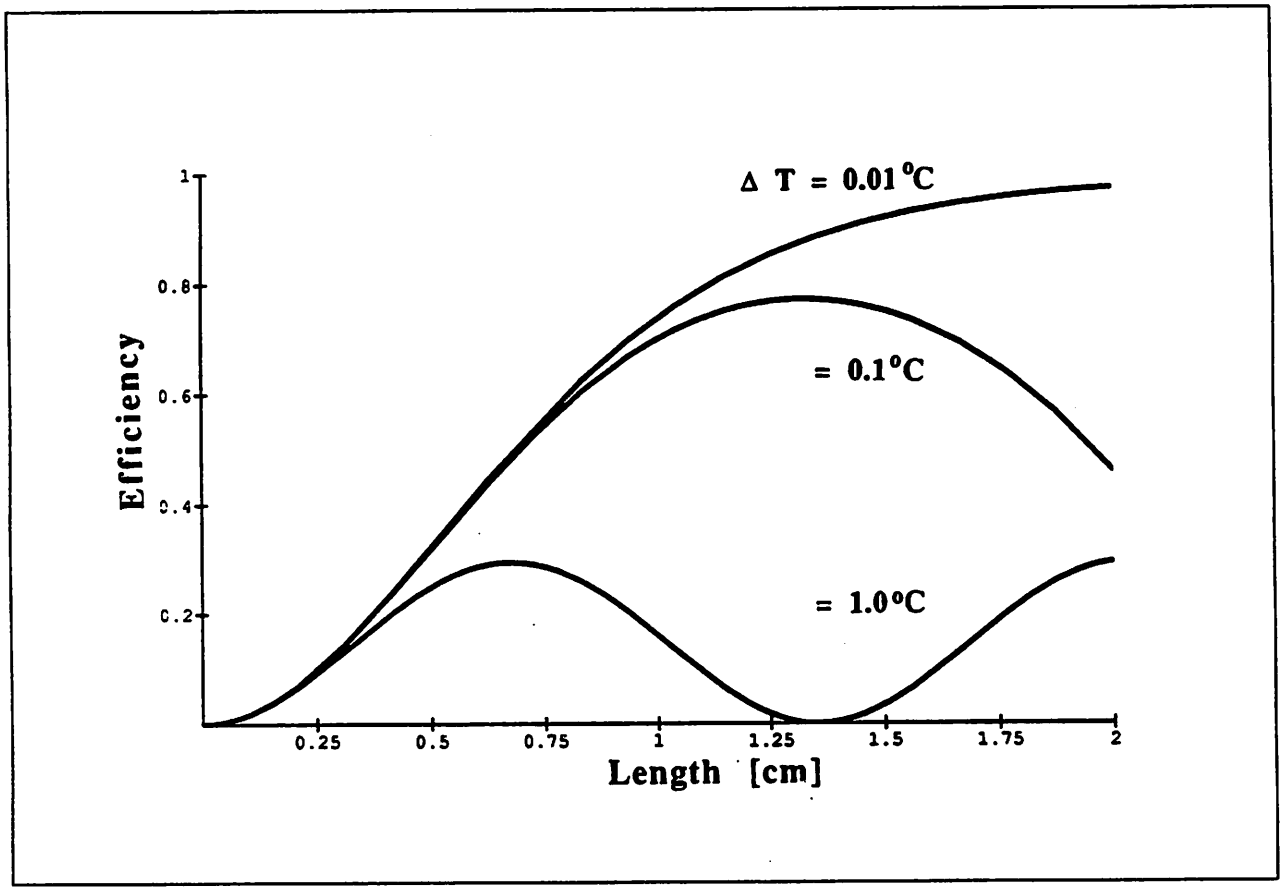

Figure 6: NCPM KD*P doubler for second harmonic with different temperature differentials.

5 Balancing

The primary goal of the nonlinear optics is to achieve the highest possible conversion efficiency in converting the fundamental Nd^+:YAG frequency into the fifth harmonic frequency. This goal is not achieved by simply maximizing the conversion efficiency of each doubling or mixing stage. Instead the conversion efficiencies of the various stages must be balanced in order to achieve overall maximum conversion efficiency. This can be illustrated by an extreme case. If, in scheme B, the conversion efficiency of the first crystal is 100%, then the overall conversion efficiency drops to 0%. Since no power remains in the first harmonic to combine with the second harmonic in the second crystal, there is no generation of the third harmonic which is necessary to the generation of the fifth harmonic. Thus if too much power is removed from any of the important lower harmonic frequencies, the efficiency of the overall system may be degraded. In order to determine the optimum power balancing, the balancing relationships for each of the two possible schemes is derived. Once the power balancing requirements are known for each of the schemes, the efficiencies of the individual crystals can be calculated and the balancing taken into consideration to decide which of the two possible schemes will give the maximum overall conversion efficiency.

There are two types of relations which are needed in order to derive the power balancing relations. The first type is the nonlinear power equation, and the second type is the conservation of power equation.

The nonlinear power equations for frequency doubling [Yariv 89, page 393] show that the power generated in the second harmonic is proportional to the input power squared. The nonlinear power relation for frequency mixing [Yariv 89, page 427] shows that the power generated in the highest frequency is proportional to the power in each of the input frequencies. In both cases the proportionality constants are dependent on the frequency, the nonlinear coefficient, the indices of refraction, and the crystal geometry. It must be noted that these nonlinear relations are approximations, used in this case to enable a good estimate of the balancing. At high efficiencies this approximation is no longer accurate, since the pump depletion is neglected. For a rigorous treatment of this problem at high intensities, the Jacobian formulation should be applied and solved with numerical techniques.

The conservation of power relations follow from the well known conservation of energy principle. Assuming no power loss within the crystal, the total amount of power exiting the crystal is the same as the total power entering the crystal.

The power balancing for the harmonic generation scheme using the fourth har-

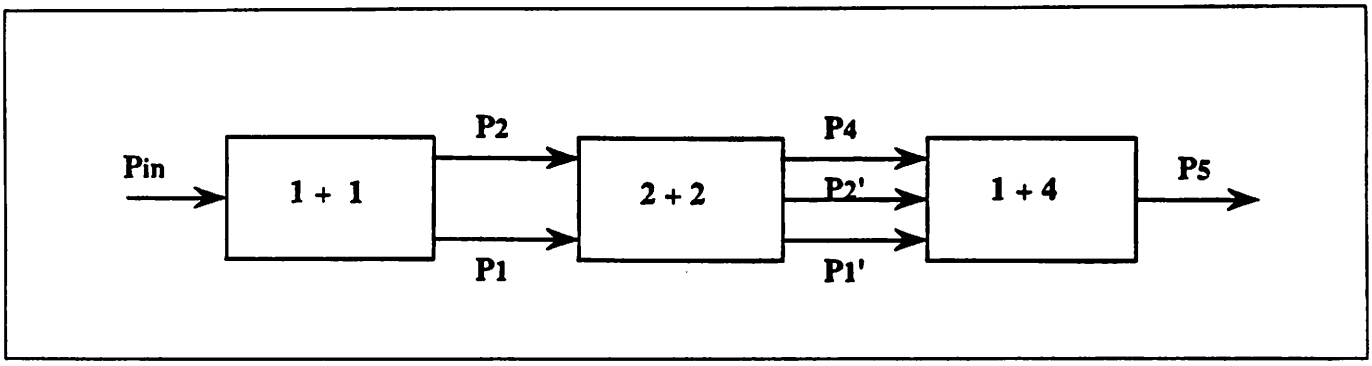

Figure 7: Definitions for the $1 + 4 \rightarrow 5$ scheme for fifth harmonic generation.

monic is straightforward, depending only on the conversion efficiency of the first crystal. The following definitions are needed in the derivation: P_{in} is the input power into the first crystal, P_1 is the power remaining in the first harmonic after the first crystal, P_2 is the power in the second harmonic, P_1' is the power remaining in the first harmonic after the second stage, P_2' is the power remaining in the second harmonic after the second stage, P_4 is the power in the fourth harmonic, and lastly P_5 is the power in the fifth harmonic. Figure 7 is a block diagram illustrating these power definitions.

The power relation is derived by utilizing the three nonlinear relations, one for each of the three crystal stages.

$$\begin{aligned} P_2 &= c_1 P_{in}^2 \\ P_4 &= c_2 P_2^2 \\ P_5 &= c_3 P_1' P_4 \end{aligned}$$

Two conservation of power relationships are also needed in the derivation. The first describes the power conservation of the first crystal, while the second is a statement of the premise that none of the first harmonic power is lost when passing through the second crystal.

$$\begin{aligned} P_1 &= P_{in} - P_2 \\ P_1' &= P_1 \end{aligned}$$

The above five equations are used to obtain the expression for the output power in the fifth harmonic, P_5, in terms of the input power, P_{in}, and the nonlinear constants c_1, c_2, and c_3. The equation thus obtained is

$$P_5 = c_1^2 c_2 c_3 P_{in}^5 (1 - c_1 P_{in}). \tag{18}$$

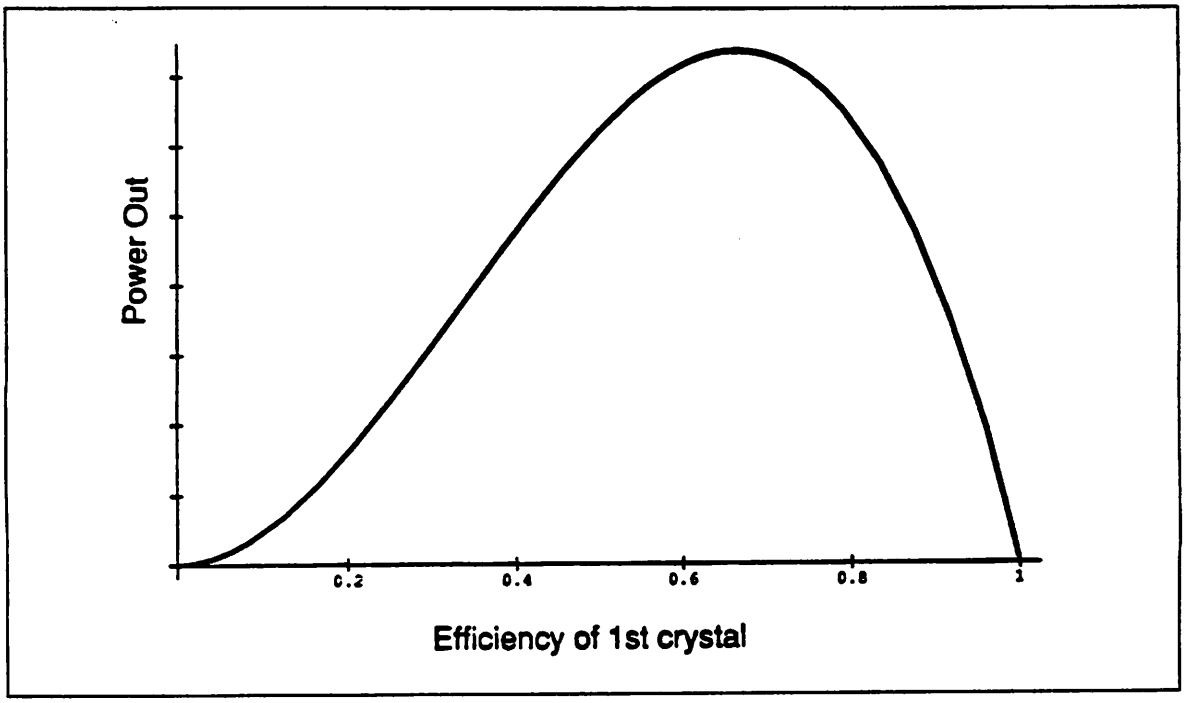

Figure 8: Power balancing relationship for the $1 + 4 \rightarrow 5$ scheme.

In order to relate this equation to the efficiency of the first crystal, we must make use of the nonlinear power relation of the first crystal again. By dividing both sides of the equation by P_{in}, we can see that the right hand side becomes the conversion efficiency of the first crystal ϵ.

$$\frac{P_2}{P_{in}} = c_1 Pin = \epsilon$$

Next substitute this relation into equation for P_5 to obtain the final form of the equation.

$$P_5 = \epsilon^2 c_2 c_3 P_{in}^3 (1 - \epsilon) \tag{19}$$

From the graph of P_5 vs. ϵ, Figure 8, notice that the output power increases with increasing conversion efficiency of the first crystal, until reaching a maximum of about 65%. After this point, the conversion efficiency of the system drops rapidly to 0% as the available first harmonic power diminishes and the mixing reaction in the third stage is depleted. Thus we should strive to get a conversion efficiency in the first crystal as close to, without exceeding 65% as possible. In practice it is quite difficult if not impossible to reach 65% efficiency, so this system is limited by the achievable efficiency of the crystals rather then the power balancing. In this scheme for fifth harmonic generation, the second stage efficiency should be maximized for generation of the fourth harmonic, since any power remaining in the second harmonic is wasted.

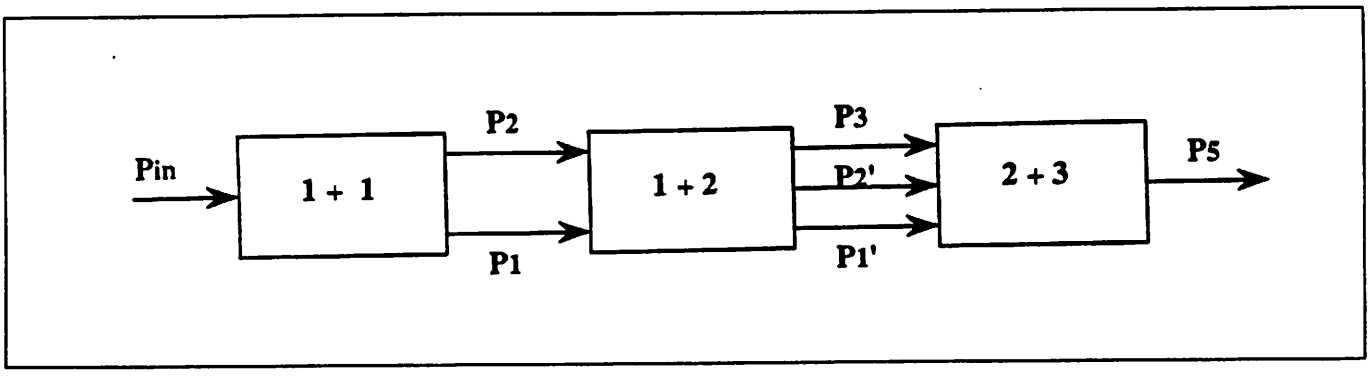

Figure 9: Definitions for the $2 + 3 \rightarrow 5$ scheme for fifth harmonic generation.

The last stage should also be maximized as the only harmonic of interest is the fifth harmonic.

The power balancing for the scheme utilizing the third harmonic is more complex than the scheme using the fourth harmonic since the fifth harmonic power is dependent on the conversion efficiencies of both the first and second crystals. For deriving the power balancing relations for the second scheme, we will use the following definitions illustrated in Figure 9: P_{in} is the total incident power, P_1 is the power in the first harmonic after the first stage, P_2 is the power in the second harmonic after the first stage, P_1' is the power left in the first harmonic after the second stage, P_2' is the power left in the second harmonic after the second stage, P_3 is the power in the third harmonic, P_5 is the power in the fifth harmonic.

The three nonlinear power relations describing the interactions in the three crystal stages are:

$$\begin{aligned} P_2 &= c_1 P_{in}^2 \\ P_3 &= c_2 P_1 P_2 \\ P_5 &= c_3 P_3 P_2'. \end{aligned}$$

The conservation relation describing the power flow in the first crystal is

$$P_1 = P_{in} - P_2.$$

The final conservation relation encompasses two ideas. The first concept is that the power remaining in the second harmonic after the second stage is equivalent to the initial power in the second harmonic minus the amount of power from the second harmonic converted into the third harmonic. This idea shown in equation form is

$$P_2' = P_2 - (\textit{fraction of power contributed by } P_2)\, P_3.$$

The second concept deals with the idea that one photon in the first harmonic (ω_1) and one photon in the second harmonic (ω_2) are annihilated to create one photon in the third harmonic (ω_3) [Yariv 89, §17.6]. We can look at this idea from the perspective of individual photon energies. We can write this as

$$\hbar\omega_3 = \hbar\omega_1 + \hbar\omega_2.$$

Substituting the knowledge that ω_2 is just twice the frequency of ω_1, since we are doing second harmonic generation, we can see

$$\hbar\omega_3 = \hbar\omega_1 + 2\hbar\omega_1.$$

Rewriting in terms of energies we obtain

$$E_3 = E_1 + 2E_1.$$

From these relations we can conclude that 2/3 of the energy in the third harmonic is contributed by the second harmonic. The final conservation relation is thus

$$P_2' = P_2 - \frac{2}{3}P_3.$$

Combining the above nonlinear and conservation power relations we can solve for P_5 in terms of P_{in} and the nonlinear constants c_1, c_2, and c_3. The resulting equation is

$$P_5 = c_1^2 c_2 c_3 P_{in}^5 [1 - c_1 P_{in}][1 - \frac{2}{3}c_2 P_{in}\,(1 - c_1 P_{in})\,]. \tag{20}$$

This relation can be simplified by letting

$$\begin{aligned} \alpha &= c_1 P_{in} \\ \beta &= c_2 P_{in}. \end{aligned}$$

The final equation is

$$P_5 = c_3 \alpha^2 \beta P_{in}^2 [1 - \alpha][1 - \frac{2}{3}\beta(1 - \alpha)]. \tag{21}$$

In order to relate the above equation to the conversion efficiencies of the first and second crystals, we must look back at the first nonlinear power relation. Dividing both sides of the equation by P_{in} and recognizing the definition of α in the result, we can obtain the conversion efficiency of the first crystal, ϵ_1.

$$\frac{P_2}{P_{in}} = c_1 P_{in} = \alpha = \epsilon_1. \tag{22}$$

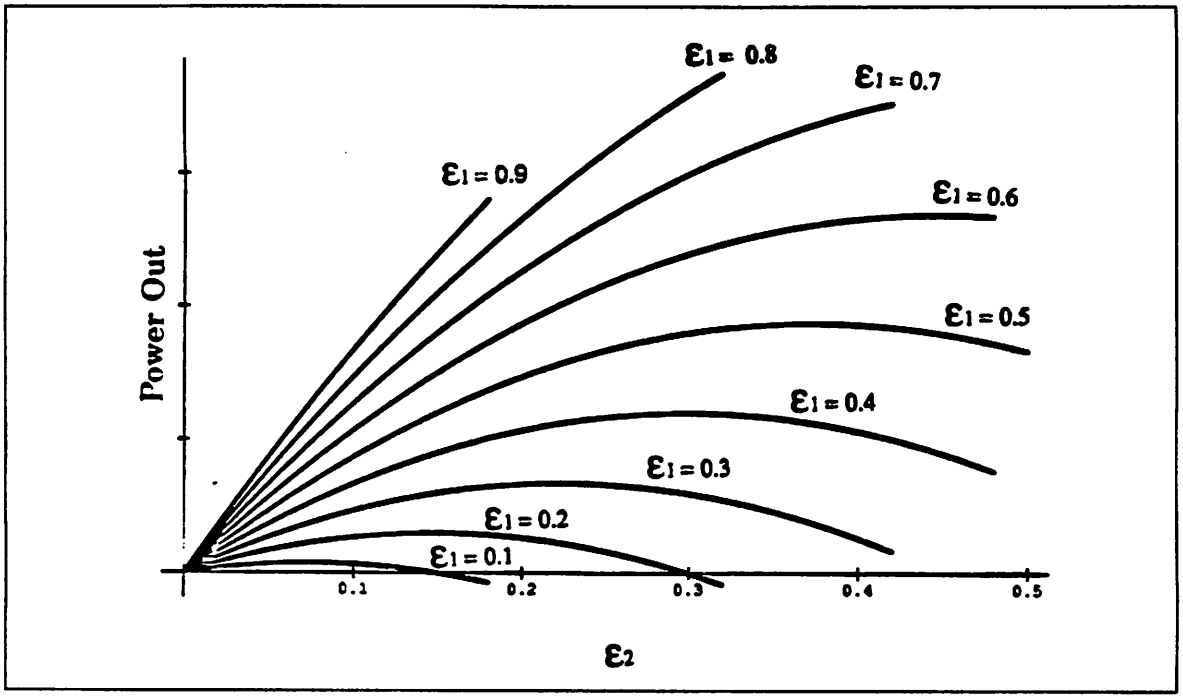

Figure 10: Power balancing relationships for the $2 + 3 \rightarrow 5$ scheme.

Relating α and β to the conversion efficiency of the second crystal is a bit more complex. Use the nonlinear power relation for the second crystal and substitute in α and β to obtain

$$P_3 = c_2 \alpha P_{in}(P_{in} - \alpha P_{in}).$$

Noting that the power incident on the second crystal is equivalent to the power incident on the first crystal we can obtain the efficiency of the second crystal by dividing both sides of the above equation by P_{in}.

$$\frac{P_2}{P_{in}} = \beta\alpha(1 - \alpha) = \epsilon_2 \tag{23}$$

Figure 10 is a parametric plot of the total power in the fifth harmonic as a function of the conversion efficiency of the second crystal (ϵ_2). Each curve is for a different value of the conversion efficiency of the first crystal (ϵ_1).

From these curves an interesting limitation can be observed. For a given first stage efficiency there is an optimum second stage efficiency. The system efficiency increases with increasing efficiencies in the first crystal. The optimum second stage efficiency arises from the fact that the second harmonic is required in the third stage to create the fifth harmonic. If the efficiency of the second stage is too high, the second harmonic will be depleted and not enough will be left over to have reasonable conversion

in the third stage. For a system with a low efficiency first stage the balancing can be a significant limitation in the overall system efficiency. This limitation will become apparent in any case where the second stage happens to have a higher maximum conversion efficiency than the first stage. To obtain the highest system efficiency the second stage must be actually be detuned to have a lower efficiency than the first stage. The conversion efficiency should be maximized in the third stage, since the production of the fifth harmonic is the goal.

6 Design Comparisons

There are a variety of approaches to fifth harmonic generation from the fundamental Nd^+:YAG frequency. To select a "best" or "optimum" approach the system constraints must be addressed. The system efficiency depends on the attainable efficiency of each stage; the polarization requirements for the desired type of phase matching; and the power balancing between harmonics. Figure 11 and Figure 12 map out the design possibilities for the $1+4 \rightarrow 5$ and the $2+3 \rightarrow 5$ schemes. The first column in both figures illustrates the three highest efficiency crystals available for the doubling stage. The middle column shows the possibilities for the second stage. In Figure 11 two doubling crystal choices are shown, one is noncritically phase matched KD*P and the other choice is a relatively low efficiency BBO type I crystal. In Figure 12 there are also two choices for the second stage illustrated. One is a very high efficiency KD*P type II crystal, and the other is a lower efficiency BBO type III crystal. The final column in both figures illustrates the only reasonable choice for their respective interactions. Once the crystal choices have been laid out, the polarization requirements of each of the harmonics and their orientation with respect to each other must be considered. The n_o and n_e axes of the crystals are labeled and the necessary orientation of the different harmonics are also labeled.

6.1 Polarization Effects

An interesting polarization effect, intrinsic to the type II doubling crystal, limits the amount of useful power in the first harmonic. As was discussed before, the type II phase matched crystal needs one wave polarized along the n_o axis and one wave polarized along the n_e axis. In the case of a doubling crystal, the input wave can be circularly polarized or linearly polarized oriented at 45° to the n_o and n_e axes for type II phase matching [Mach. 76]. The generated second harmonic will propagate along the n_e axis, and the first harmonic output power will be evenly split along the two

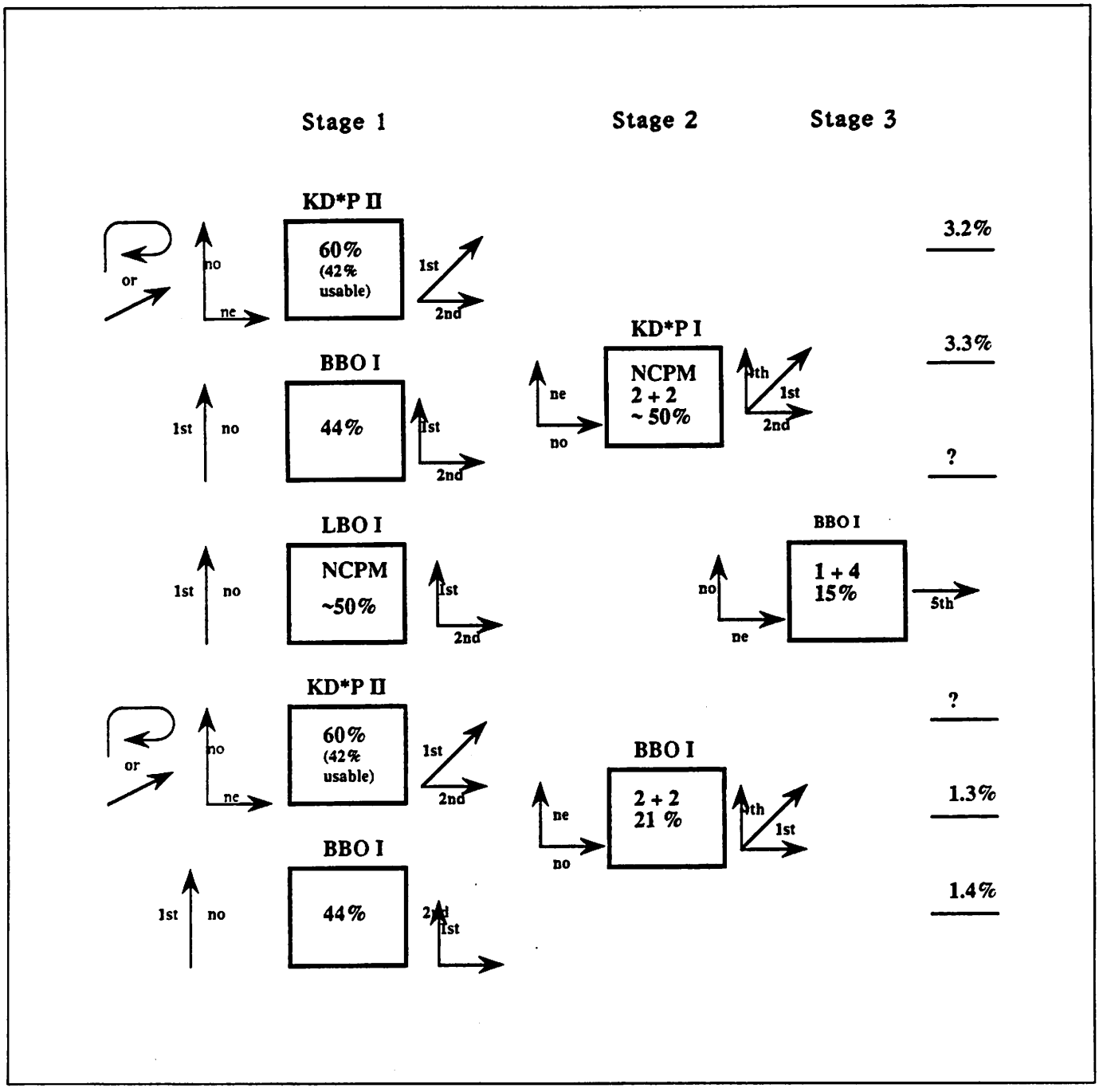

Figure 11: Possible $1 + 4 \rightarrow 5$ schemes illustrating crystal choices for each stage and polarizations of the harmonics.

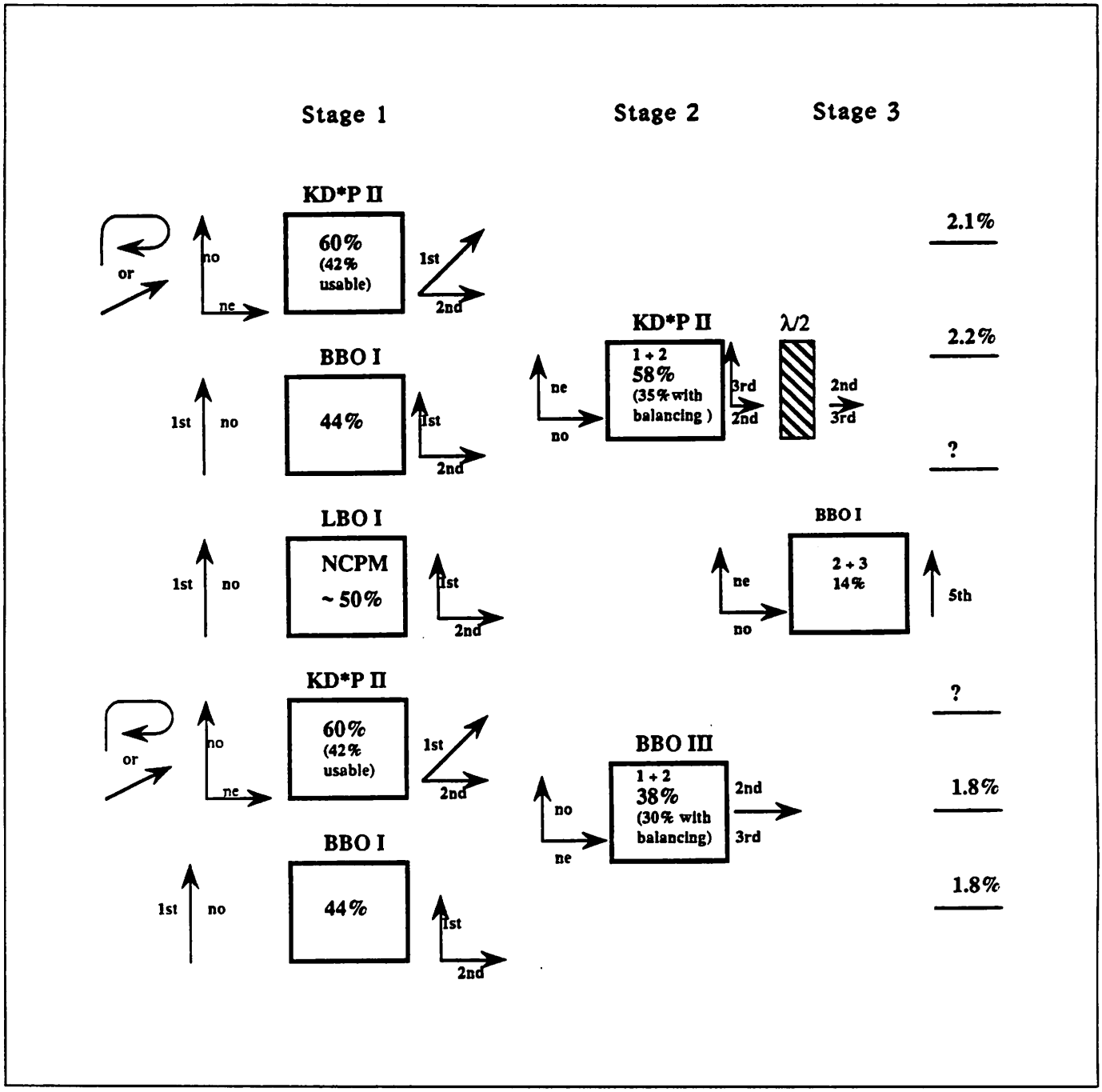

Figure 12: Possible $2 + 3 \rightarrow 5$ schemes illustrating crystal choices for each stage and polarizations of the harmonics.

axes. In the absence of exacting length and temperature data the prediction of the polarization of the first harmonic exiting the doubler crystal is impossible to predict. Because the crystal itself is a highly birefringent material, it will act as a waveplate. The final polarization depends on the thickness of the crystal and an immeasurably small change in the thickness of the crystal will change the final polarization. The important result of this waveplate action is that the fundamental beam will have its power split along the two axes and it is not possible to rotate it to be polarized along one axis or the other with respect to the generated harmonic since the polarization is unknown. This will limit the power available in the first harmonic at later stages. Only 71% of the first harmonic power, remaining after the doubling stage, will be usable. For this reason the apparently less efficient type I BBO crystal actually has a higher effective efficiency for the system as a whole. This problem does not extend to mixing crystals, since the different frequency waves are linearly polarized, aligned with only one of the n_o or n_e axes.

6.2 Design Options

Keeping the system constraints for this particular design in mind, consider the 1+4 → 5 quintupling scheme, illustrated in Figure 11, in more detail. The first stage crystal choices are the KD*P type II doubler, the BBO type I doubler or the NCPM LBO type I doubler. Due to the waveplate effect described above, the KD*P and the BBO crystals have nearly equivalent conversion efficiencies. The BBO crystal is a more robust material in terms of optical damage and heating tolerance. The third crystal LBO is very attractive alternative since it has potentially very high efficiencies as it is a noncritically phase matched interaction. A high quality LBO crystal is unfortunately difficult to obtain at this time. In the future, as alternative sources of LBO crystals become available, it would likely be a clear choice for this application. The two second stage choices are either a KD*P NCPM crystal or a low efficiency BBO type I crystal. The BBO crystal is a poor choice because of its low conversion efficiency. There are questions about the benefit of using the noncritically phase matched crystal for this high average power application. If the KD*P crystal suffers absorption, the heating could increase the phase mismatch, reducing the efficiency. For the third and final stage the type I BBO crystal is the obvious choice, since the alternative has unacceptably low efficiency. For this scheme of quintupling, the power balancing is not an issue since the first crystal conversion efficiency is well below the threshold for power depletion.

For the quintupling scheme illustrated in Figure 12, the first stage considerations are the same as those described in Figure 11. The second stage is a mixing stage and there are two choices apparent for this interaction. The type III crystal has an

advantage of allowing the polarizations of the second and third harmonics to be parallel and thus no waveplate will be needed for the system. The drawbacks to using this crystal are two-fold. This crystal has much lower efficiency, and additionally this interaction requires a very long crystal which is expensive and prone to heating problems. The second possible crystal is a KD*P type II mixer. This crystal is very attractive as it is a well known material with very high conversion efficiency. For the third and final stage, there is only one crystal, a BBO type I mixing crystal. An additional consideration for the scheme using the 3rd harmonic is power balancing. Power balancing has a significant effect on this system, since the calculated efficiency of the second stage is much higher than that of the first stage. Unfortunately the power balancing requires the second crystal to have slightly lower efficiency for optimum system conversion efficiency (see §5). In this case the second crystal must be detuned in order to increase system conversion efficiency. Thus, a high first crystal efficiency is vital to a high efficiency system. If the first crystal efficiency could be increased, the second crystal would not need to be as drastically detuned and the total system efficiency would increase.

These design configurations omit an important consideration, heat flow management. Methods for dealing with this additional constraint are discussed in the following section.

7 Beam Compression Optics

There are two purposes for compressing the output light from the Nd^+:YAG laser source. The first reason is simply to increase the peak power density while not significantly increasing the angular divergence of the beam in the angularly sensitive direction. The second reason for beam compression is to improve heat flow, thus reducing the temperature-induced phase mismatch. The design of the optics, to accomplish beam compression depends heavily on the specific system under consideration, since the divergence matching of the particular stages and/or the dispersion of different harmonic frequencies must be addressed.

7.1 Power Density

Generally the benefit derived from homogeneously compressing the input beam to increase the peak power density is counteracted by the increased divergence caused by the focusing. The increased divergence detracts from the the phase matching,

reducing the conversion efficiency, by exactly the same factor as the increased power from symmetric beam compression increases the conversion efficiency. The net effect is that for higher power density a shorter crystal is needed to regain the original conversion efficiency. But if the compression is done in only one direction, in particular the direction less sensitive to angular divergence, we can increase the power density without increasing the divergence and thus derive a net benefit. The n_o direction is the nonsensitive direction because the index of refraction is constant with respect to the angle of propagation along the n_o direction. One problem which is evident with this method, is that the nonsensitive direction for a particular stage is not necessarily parallel to the nonsensitive direction of the preceeding stage. These problems will be further discussed in the design of the beam compression optics.

7.2 Heat Flow Management

One of the motivations for redesigning the nonlinear optics is to improve heat management. In the current low average power system, heating problems are revealed in the BBO fifth harmonic crystal [Partlo 92]. In the new higher average power system, heating is expected to be a critical issue. The precise cause of heating depends on the crystal in question. For KD*P the absorption decreases with the amount of deuteration, but the crystal cannot be 100% deuterated, so some residual absorption may cause problems at high average powers. In BBO the source of the absorption is unknown, but whatever the cause, heating is a significant problem at high average powers. Temperature differences across the face of the nonlinear crystal will cause changes in the index of refraction which in turn alter the phase matching conditions. The temperature difference causes the crystal to be correctly phase matched over only a portion of the crystal area, thus reducing the crystal's conversion efficiency. Since the crystal is a very good insulator the temperature difference cannot be affected by heating the crystal in an oven. Maintaining the average crystal temperature is important for stability, but the temperature profile within the crystal can only be changed by changing the crystal geometry. The heat flow in two general geometries, the rod and the slab, were examined.

The temperature profile in an infinite rod with radius a is described by the following equation from [Carslaw 59]

$$T = \frac{P_{in}\alpha}{4\pi k a^2}(a^2 - r^2), \tag{24}$$

where the temperature T, due to the absorption in the volume of the solid, as a function of radial position r is given in terms of P_{in} the incident power, α the absorption

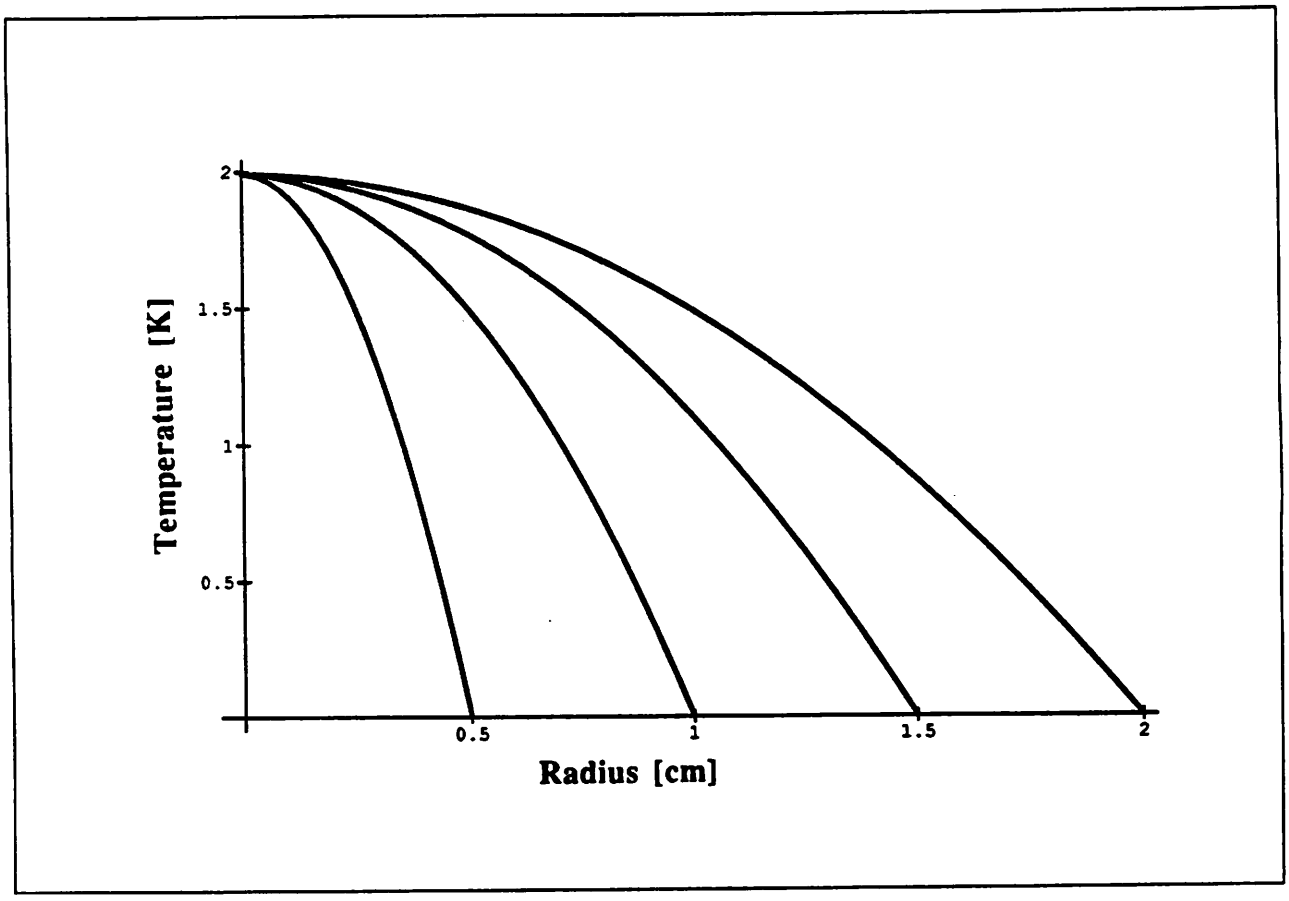

Figure 13: Temperature profile of an infinite rod.

coefficient, and k the conductivity of the material. The rod is assumed to be infinite in length, have the outside surfaces maintained at a constant temperature (0°K in this case), and have volumetric heating at a constant rate due to absorption. The resulting temperature profiles for rods of different radii are graphed in Figure 13. Note that the center temperature is constant with respect to the radius of the rod, as can also be seen by looking at the above equation when $r = 0$.

$$T = \frac{P_{in}\alpha}{4\pi k} = constant. \tag{25}$$

Since altering the rod geometry has no effect on the temperature differential, the temperature difference between the center and the edge of the rod, the rod geometry does not offer any improvement in reducing the phase mismatch. We can only change the gradient not the magnitude of the temperature differential.

Since the rod geometry does not allow for improved management of heat flow, an alternative geometry is examined. The heat flow in an infinite slab with thickness t

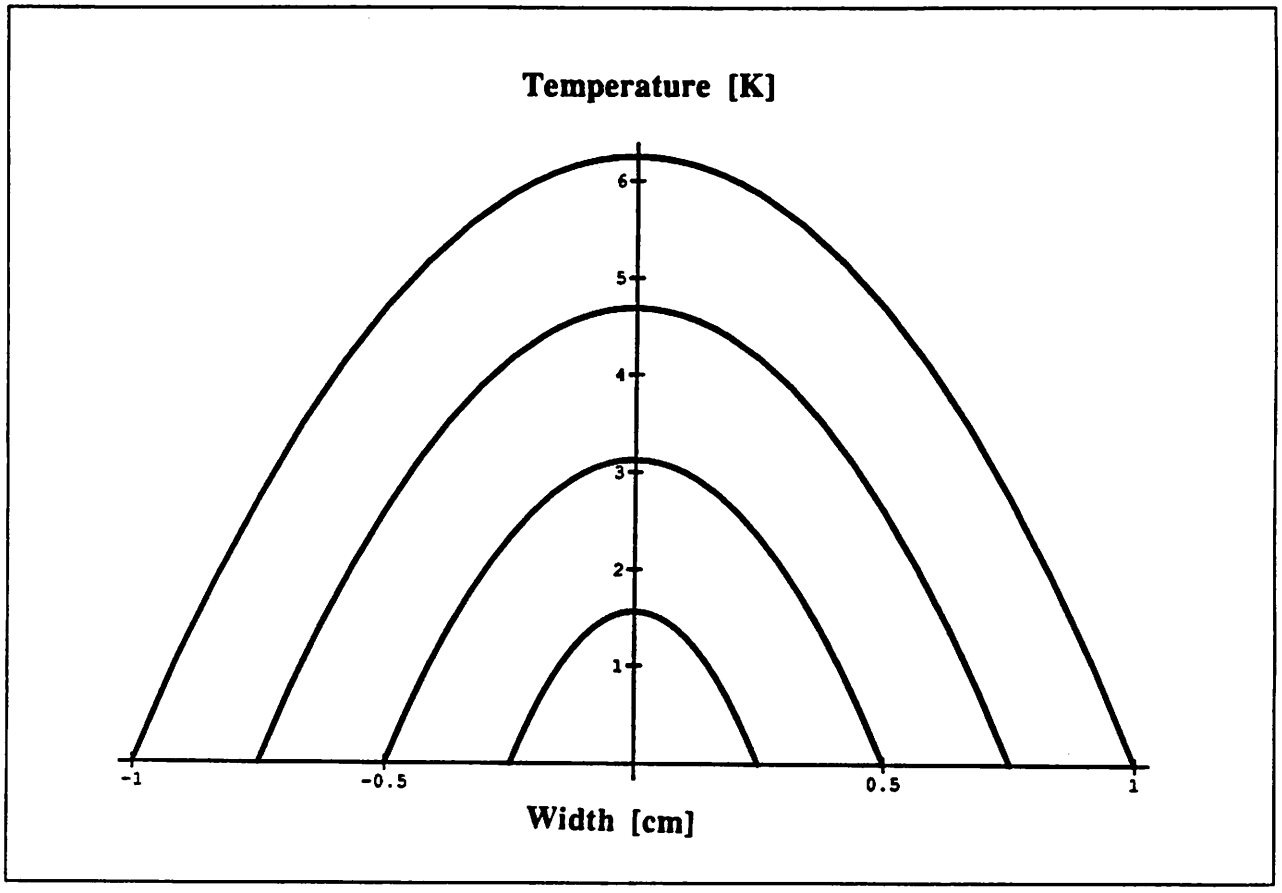

Figure 14: Temperature profiles for infinite slabs at various widths.

---

and width L [Carslaw 59] can be given by

$$T = \frac{P_{in}\alpha}{4ktL}(L^2 - x^2), \tag{26}$$

where P_{in} is the incident power, α is the absorption coefficient, k is the conductivity, and x is the displacement in the width direction. The temperature profiles of slabs with different widths are shown in Figure 14. To obtain the information of interest, we again look at the variation of the center temperature with respect to the geometry of the solid.

$$T = \frac{P_{in}\alpha}{4k}(\frac{L}{t}),\ x = 0 \tag{27}$$

This result shows that the center temperature is dependent on the geometry of the solid. The center temperature is linearly dependent on the thickness of the slab for a slab of constant width. From this result we see that we can improve the temperature differential across the crystal face by increasing the aspect ratio.

In conclusion, the heat flow equations reveal that a slab geometry is preferable for reducing the phase mismatching in the crystal due to temperature variations across the crystal face. In the new harmonic generator quintupling system we plan to aim for a compression ratio of 3:1 to 4:1, which must match the aspect ratio of the nonlinear crystals in order to fill the crystal with the input beam. The precise ratio will be determined by the limitations of the beam compression optics which are described in detail in the following section.

7.3 Design of Beam Compressor

The design and positioning of an appropriate beam compressor depends upon the relative orientations of the polarizations of the angularly sensitive axis after each nonlinear stage in the harmonic generator. A system in which the beam compressor can be placed in front of the first stage is preferable, although it is clear from Figure 11 and Figure 12 that the sensitive and nonsensitive axes are seldom conveniently aligned. When the beam compressor can be placed before the harmonic generator, all three stages derive the benefit of improved heat extraction and higher peak power, and the additional complication of dealing with more than one frequency can be avoided. Even with the stringent polarization requirements there are several case where the beam compressor can be placed prior to the nonlinear optics. For example consider the scheme in Figure 12, if the first harmonic beam is compressed, the second stage, which is highly efficient, may still give acceptable conversion even with the increased divergence of the first harmonic. An alternative to accepting the divergence mismatch is to design a waveplate to rotate both beams by 90 degrees, in effect reorienting the polarizations into the optimum position. A third design which allows for the beam compressor to come before the harmonic generator utilizes a noncritically phase matched (NCPM) crystal as a doubler. For a system with a NCPM crystal, both directions are non-sensitive. This additional degree of freedom reguarding beam compression is an additional reason for interest in noncritically phase matched crystals. In particular, the LBO NCPM doubling crystal is an attractive option. In some cases however, the beam compressor must be placed after the first nonlinear stage. In this situation the dispersion of the two different frequency beams becomes an important consideration. The same basic beam compressor may be used in either position, but some designs may require additional components to rotate the polarizations to the proper positions.

The beam compressor consists of one or more right angle prisms. The prism is designed so the light enters along the surface normal of one side of the prism, and exits the slanted side, refracted at large angle compressing the beam in the process. The prism is illustrated in Figure 15. The beam enters the prism normal to the surface in

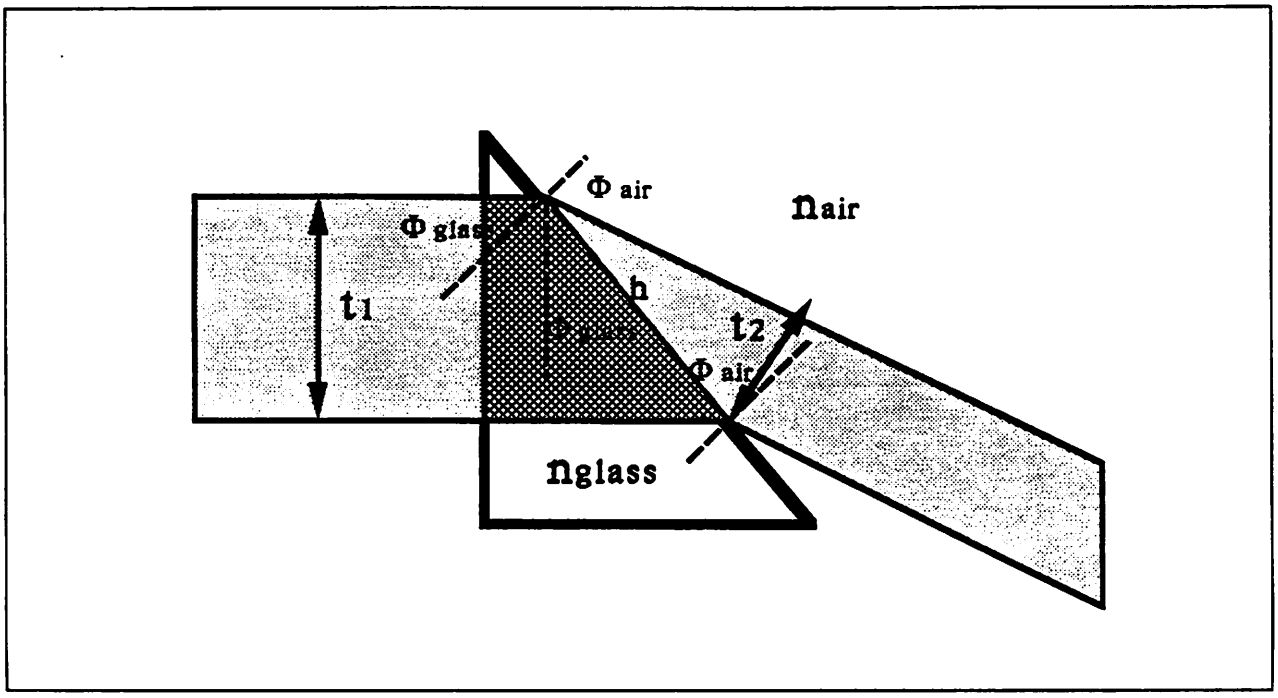

Figure 15: Single prism beam compressor.

order to minimize the surface reflection loss. The prism is cut so that the rays will exit at Brewster's angle which essentially eliminates reflection losses at the back surface. At Brewster's angle one polarization has 0% reflection loss while the other polarization has significant reflection losses. Figure 16 illustrates the reflection loss versus angle with respect to the surface normal for both the R_s and R_p polarizations[Fowles 89]. The Brewster's angle is defined as

$$\theta_B = tan^{-1}(n_{glass}), \tag{28}$$

where n_{glass} is the index of refraction of the prism material. Analyzing the geometry and applying Snell's Law, the demagnification of the beam passing through the prism can be shown to be as follows

$$\frac{t_2}{t_1} = D = \frac{1}{M} = \frac{cos(\phi_{glass})}{cos(\phi_{air})}, \tag{29}$$

where t_2 is the width of the compressed beam, t_1 is the width of the input beam, M is the magnification of the beam, and ϕ_{air} and ϕ_{glass} are the angles with respect to the surface normal in the air and glass. These quantities are labelled in Figure 15.

The remaining design variable is the index of refraction of the prism material. Changing the index of refraction will alter the Brewster's angle and thus the magnification. Figure 17 is a design graph showing the magnification versus reflection

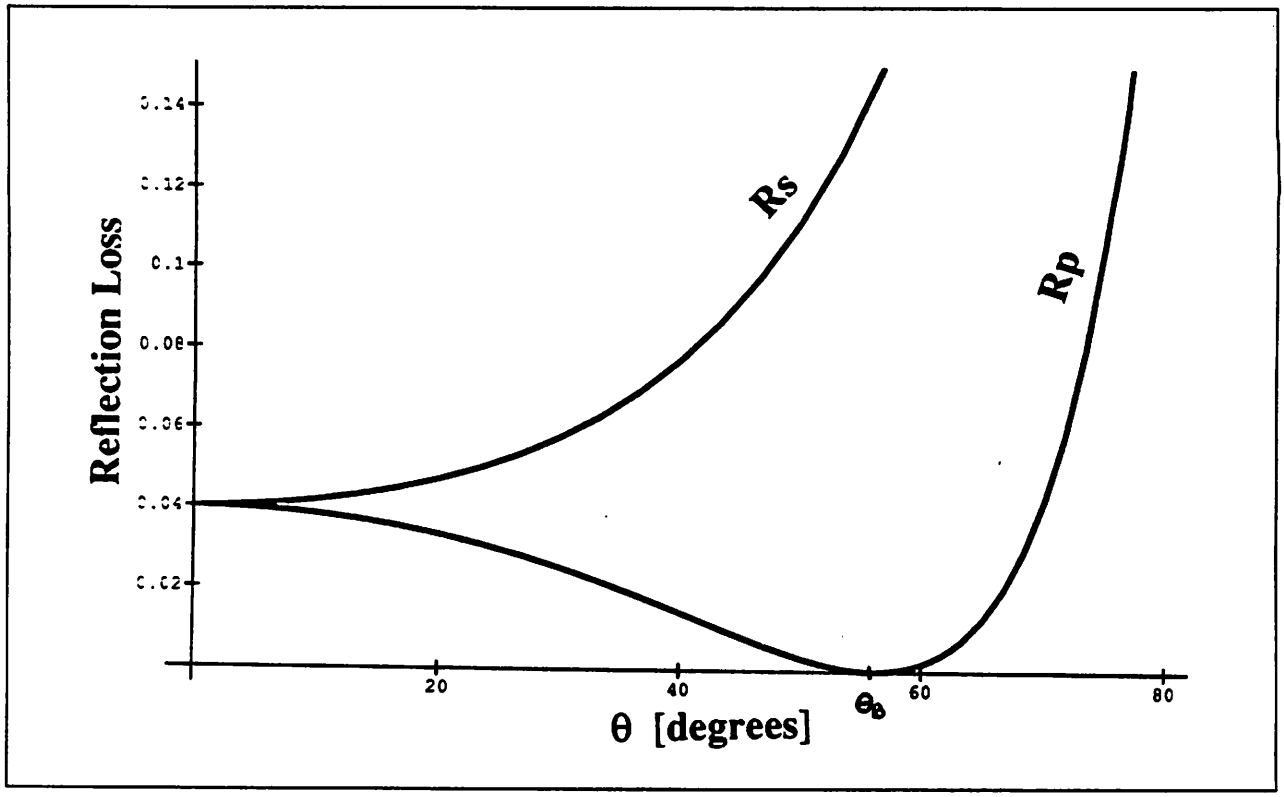

Figure 16: Reflection losses for both the R_s and R_p polarizations versus the angle of the beam with respect to the surface normal. θ_B denotes Brewster's angle.

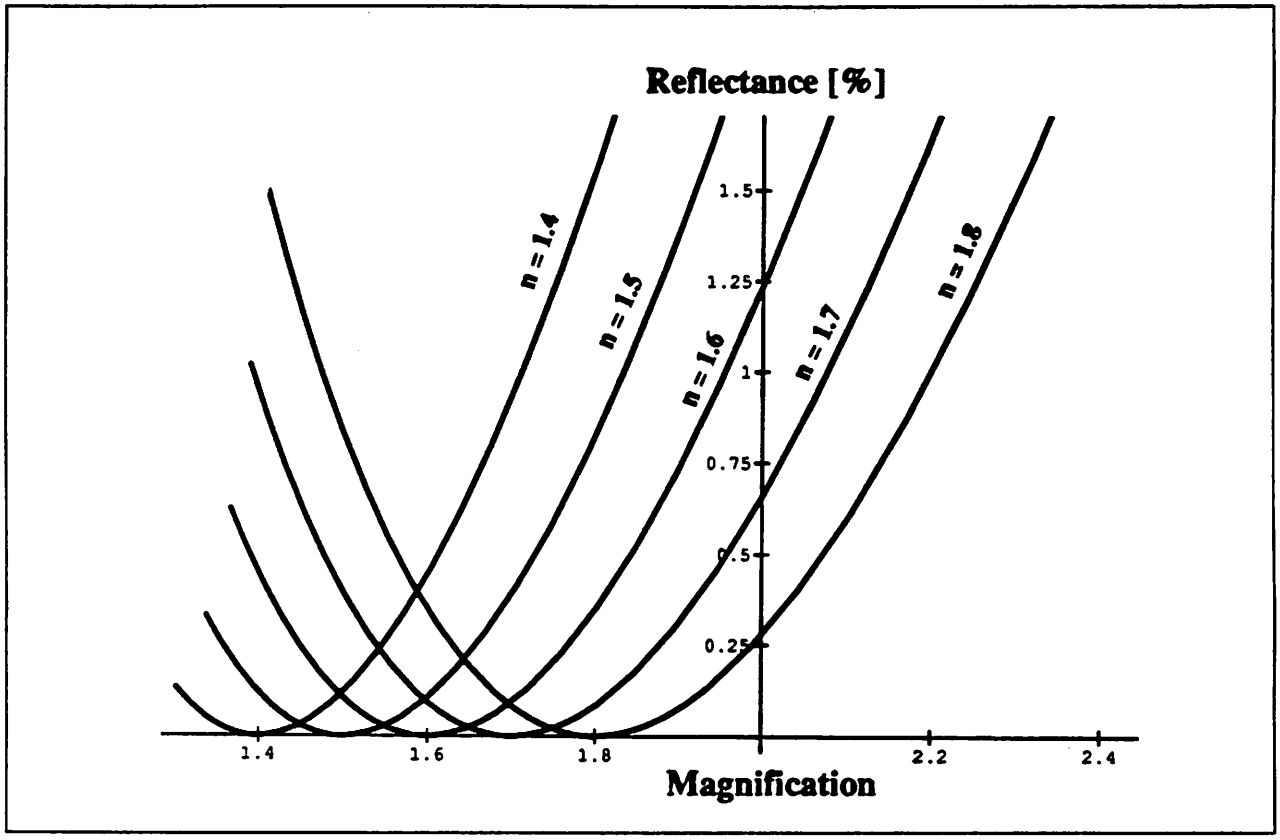

Figure 17: Design graph for single prism with varying indices of refractions and angles.

losses for different indices of refraction. The point at which the reflectance losses go to 0% indicate the beam is refracted at exactly Brewster's angle. Figure 17 indicates that the angle can deviate from Brewster's angle, changing the magnification, without great reflection losses. The magnification values indicate that two or more prisms will be required to attain the desired compression factor (3–4). If in the two-prism beam compressor, the second prism is placed inverted with respect to the first, the exiting beam will be emitted parallel to to the original beam, thus assisting in the alignment of the system as a whole. For a system in which the beam compressor is placed prior to the first nonlinear stage, a virtually lossless, two-prism, compressor can be constructed to give the desired demagnification ratio.

If the beam compression optics must be placed between the first and second stages, the presence of both the fundamental and second harmonics increases the complexity of the analysis. Since the index of refraction of the glass is frequency dependent, Brewster's angle will differ for the two frequencies. This dispersion will cause the different frequency beams to diverge, gradually reducing the overlap of the beams and

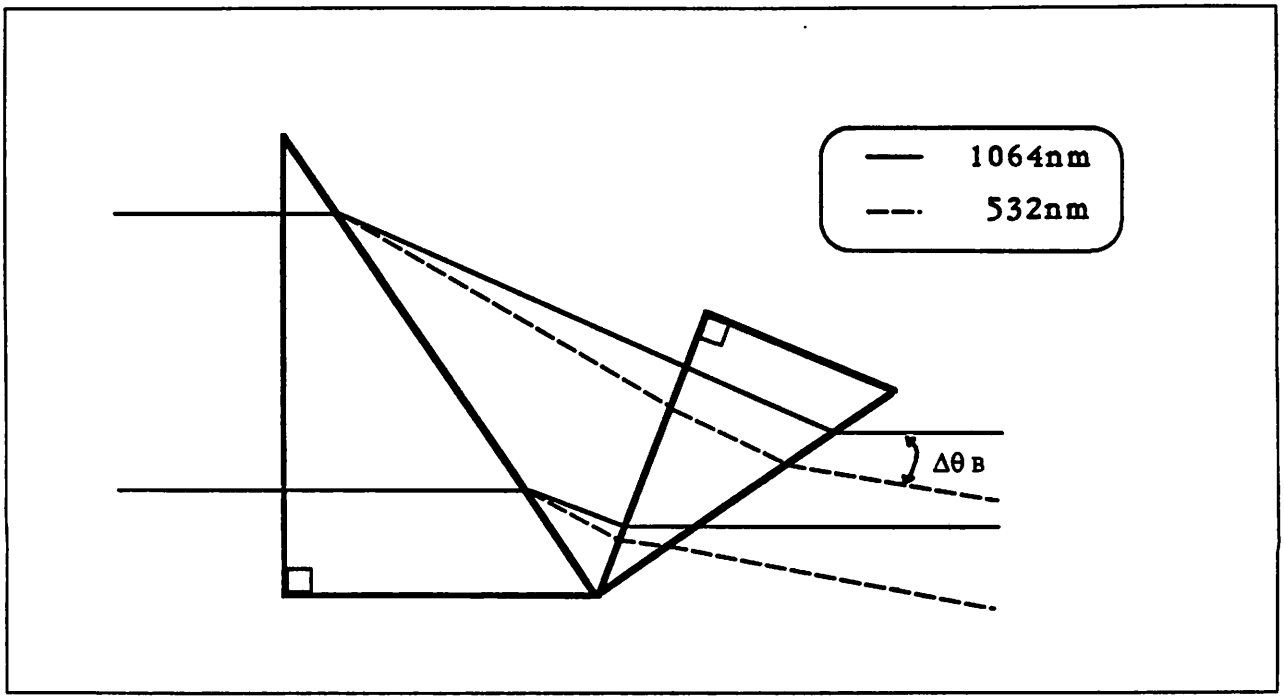

Figure 18: Two prism beam compressor.

therefore the amount of area over which the mixing interaction occurs. An additional benefit of a two-prism system is that the divergence will be less than a single prism system. The two-prism beam compressor is illustrated in Figure 18. The divergence angles are exaggerated for illustration.

The angular divergence between the fundamental and the second harmonic beams can be calculated and shown to be dependent on the difference in the index of refraction at the two frequencies Δn. Using Snell's Law, the definition of Brewster's angle and geometry, the expression for the divergence of the two beams $\Delta\theta_B$ can be shown to be

$$\begin{aligned}\Delta\theta_B &= \theta_B^{\omega_1} - \theta_B^{\omega_2} \\ &= \theta_B^{\omega_1} - sin^{-1}[(n_{glass} + \Delta n) sin[\theta_{glass} - \\ &\quad sin^{-1}[\frac{1}{n_{glass} + \Delta n} sin[sin^{-1}[sin[\theta_{glass}](n_{glass} + \Delta n)] - \theta_B]]]],\end{aligned}$$

where n_{glass} is the index of refraction of glass at the fundamental frequency, $\theta_B^{\omega_1}$ is Brewster's angle at the fundamental frequency, and $\theta_B^{\omega_2}$ is the exit angle of the second harmonic. Figure 19 shows θ_B versus Δn for three materials with different indices. SF11 is a high index glass, BK7 is a commonly used glass, and SiO_2 is fused silica. The divergence problem eliminates the use of materials with high Δn because the θ_B

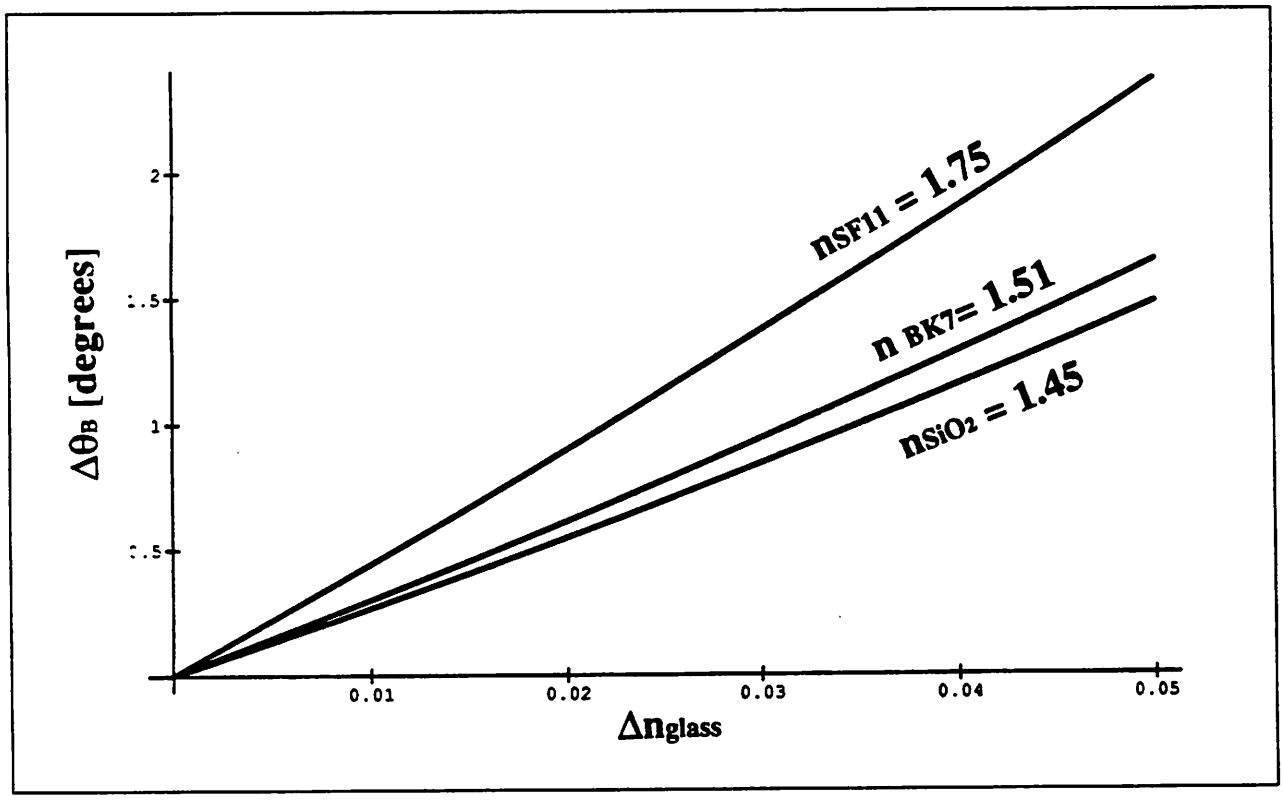

Figure 19: Graph showing divergence of beams with respect to the index of refraction difference for three materials, SF11, BK7, and fused silica.

becomes too large. For this reason, a material such as fused silica is a good choice, even though the magnification factor is lower.

It is interesting to note that the divergence for a two-prism system is lower than the divergence of a single prism system. In the first prism the divergence is caused purely by dispersion. In the two-prism system the situation is more complex. Since the two beams are traveling at different angles, the second prism can only be aligned normal to one of the beams. Assuming the surface is aligned for the fundamental frequency, the second harmonic will strike the second prism at an angle to the surface normal and be refracted inside the second prism. The beam will be bent closer to normal incidence. While the higher frequency beam will be bent more at the output face of the prism, it has a greater angle to overcome to begin with. The net effect is that the angle due to dispersion alone will be partially overcome by non-normal angle inside the prism and the divergence is reduced.

For the case where a compression ratio of 1:4 or higher is desired, three prisms may be required. A fortuitous side-effect of using three prisms is that the divergence is even further reduced. Figure 20 shows the orientation of the three-prism beam compressor and an exaggerated rendition of the divergence effects on the two frequency beams. With the third prism, the second harmonic beam will actually be over corrected causing the $\Delta\theta_B$ to be negative. Figure 21 is a graph of $\Delta\theta_B$ with respect to Δn for fused silica.

In summary, we have discussed two motivations for beam compression along one axis — increase peak power density and reduced temperature profile — and the design of a component to accomplish the task. The position of the compressor is an important issue. While it is desirable to place the beam compressor before the harmonic generation, polarization considerations may dictate placement inside the harmonic generator. Inside the harmonic generator the divergence of the fundamental and higher harmonic frequencies must be considered and minimized to avoid detracting from the conversion efficiency.

8 Conclusion

The design of a fifth harmonic generator for use with a Nd^+:YAG source laser is discussed in detail. Together the laser and nonlinear optics form a 213nm source for optical lithography capable of pattering lines and spaces as small as 0.18 microns.

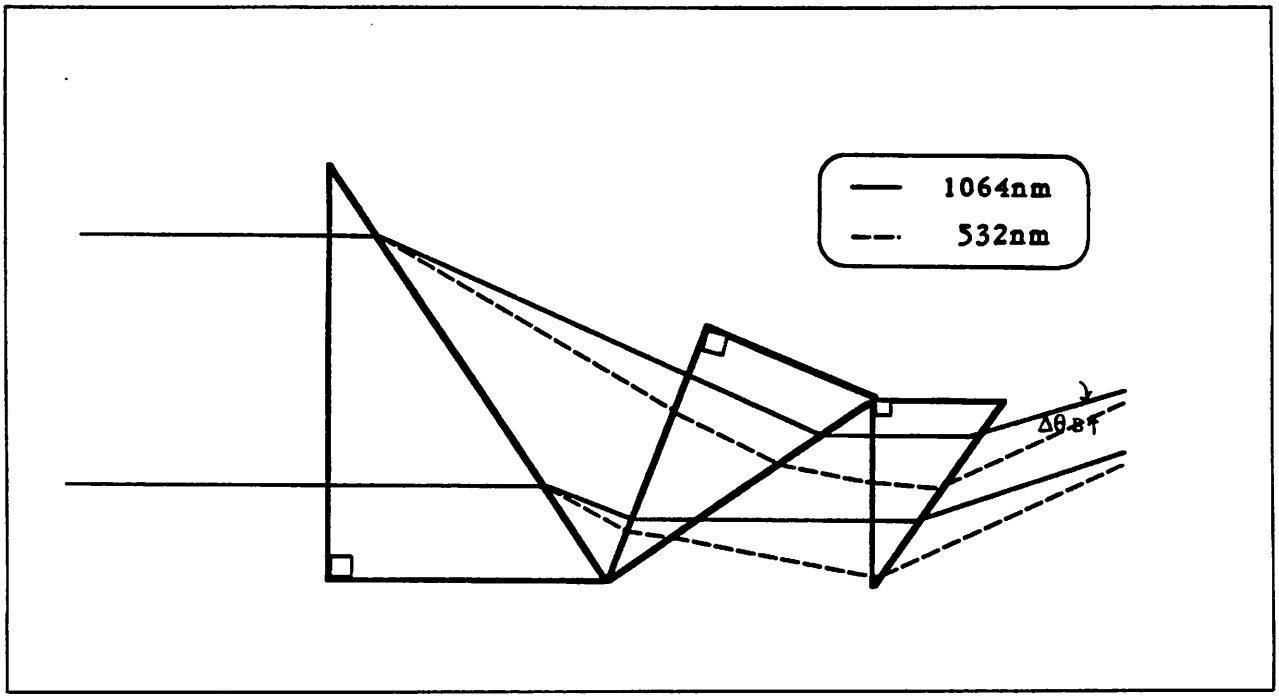

Figure 20: The three-prism beam compressor.

The design strategy for this particular system can be generalized to a design methodology for any multi-stage nonlinear optical system. The design problem can be broken down into several steps. One task is to assess the available materials eliminating those inappropriate to the particular system requirements. The nonlinear parameters need to be calculated for the frequencies, interactions, and power levels of interest, culminating in two particularly useful parameters, the nonlinear coupling parameter c and the drive η_o. Another step in the design involves using η_o and c to calculate the nonlinear conversion efficiencies for each crystal. For low efficiency crystals, the depletion or dephasing may be disregarded and a simple efficiency approximation will suffice. In situations, such as the fifth harmonic generator under consideration, where both the dephasing and pump depletion are significant, the Jacobian efficiency formula should be used. The Jacobian formulation has the additional benefit of giving an optimum length for the crystal. A first pass approximation of the power balancing can shed light on another system constraint. The balancing analysis shows that for some schemes power balancing may not be an important issue, while for other schemes balancing can be a real limiting factor and thus must be carefully considered.

By constructing a diagram which incorporates the information gathered about efficiencies, waveplate effects, balancing, and polarization requirements, a comparison

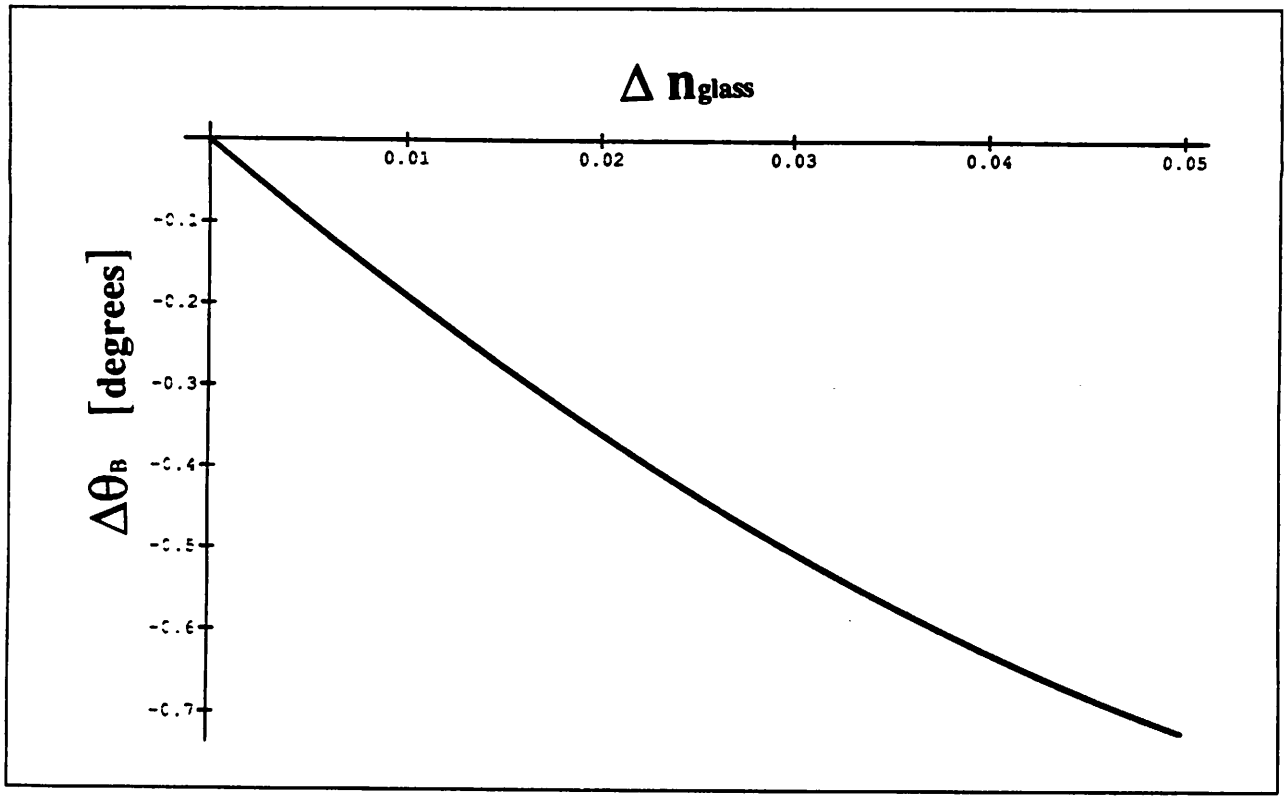

Figure 21: The divergence of the three beams with respect to the difference in the index of refraction for fused silica for the three-prism beam compressor.

can easily be made among the various fifth harmonic generation schemes. In analyzing the benefits and limitations of each scheme the additional constraint of involving heat flow is also taken into account. A slab geometry proves to have better heat flow characteristics, than the traditional rod or square geometry. In order to implement the slab geometry crystals, the beam entering the crystals must be shaped to have the same aspect ratio as the crystal slab. The polarizations within the system apply an additional constraint. Since, in order to preserve the low divergence of the beam, we wish to compress in only the nonsensitive direction for each crystal, the beam compressor needs to be carefully designed. To maintain high efficiency in the harmonic generator, the beam compressor must have low reflectivity and, if placed after the first stage, must not allow much divergence of the two frequency beams. With the design of an appropriate beam compressor, the final harmonic generator design can be completed and implemented.

For the specific application detailed in this paper, the scheme using the second and third harmonics to produce the fifth harmonic looks most promising. In this basic scheme, the BBO type I doubler is the best choice for the first stage, until the LBO NCPM doubler becomes available. The prism beam compressor would then follow the first stage with the BBO or precede the first stage with the LBO. In the position following the first stage, an appropriate use of waveplates is needed to properly orient the polarizations. The second stage will be the type II KD*P crystal since it is a clear efficiency winner. The only choice for the last stage in this scheme is the BBO type I crystal.

Future work will focus on actually implementing the fifth harmonic generator for use in optical lithographic imaging. Additional work on the theory needs to be done to more rigorously treat the balancing problem, probably by using numerical methods to solve the Jacobian formulas for the efficiencies. The practical problem of the polarization rotators for the prism beam compressor also needs to be resolved.

Acknowledgments

First and foremost I wish to thank my advisor, Professor W.G. Oldham for his patient guidance throughout this project. I would also like to thank Professor A.R. Neureuther for his assistance. I greatly appreciate the advice and comments from the researchers at Lawrence Livermore National Laboratory; Steve Velsko and Ray Beach stand out in particular. Dr. William Partlo is also deserving of thanks for providing the foundation for this work while he was a graduate student here at Berkeley. I would also like to acknowledge the assistance, in understanding the fundamentals,

given to me by Christopher Pohalski at Stanford University. Last but definitely not least, I wish to thank Anita K. Lee, the Nd^+:YAG laser half of this design project, for hours of enlightening conversations.

This project was funded by SRC/SEMATECH contract.

References

[Butcher 90] Butcher, P. N., Cotter, D. *The Elements of Nonlinear Optics.* New York : Cambridge University Press, 1990.

[Carslaw 59] Carslaw, H.S. and Jeager, J.C. *Conduction of Heat in Solids.* Oxford : Claredon Press, 1959.

[Chen 86] Chen, Chuantian. "Recent Developements in Barium Borate". SPIE Vol. 681 *Laser and Nonlinear Optical Materials* (1986).

[Eimeral 87a] Eimeral, D., "High Average Power Harmonic Generation". IEEE Journal of Quantum Electronics, **QE-23**, No. 5, p.575 (1987).

[Eimeral 87b] Eimeral, D., Davis, L., Velsko, S. "Optical, Mechanical, and Thermal Properties of Barium Borate". J. Appl. Phys. **62** (5) p. 1968 (1987).

[Eimeral 87c] Eimeral, D. "Electro-Optic, Linear, and Nonlinear Optical Properties of KDP and Its Isomorphs". Ferroelectrics, **72**, p. 95 (1987).

[Fowles 89] Fowles, G. R., *Introduction to Modern Optics.* New York : Dover Publications, Inc. 1989.

[Hon 79] Hon, D. "High Average Power, Efficient Second Harmonic Generation". *Laser Handbook.* North-Holland Pub. Co. (1979).

[Mach. 76] Machewirth, R.A., Webb, R., Anafi, D. "High Power Harmonics Produced With High Efficiency in KD*P". Laser Focus, May 1976.

[Partlo 92] Partlo, William. *Issues In Deep-UV Lithography Using Pulsed Laser Light Sources.* Ph.D Thesis, U.C. Berkeley, January 1992. Memorandum No. UCB/ERL M92/14.

[Tyminski 90] Tyminski, J.R., Frangineas, G., Reed, E., Bischel, W. "Materials for High Power Second Harmonic Generation". SPIE Vol. 1223 *Solid State Lasers* (1990).

[Ukachi 90] Ukachi, T., Lane, R.J., Bosenberg, W.R., Tang, C.L. "Measurements of Noncritically Phase-matched Second-harmonic Generation in a LiB_3O_5 Crystal". Appl. Phys. Lett. **57**(10) p. 980 (1990).

[Yariv 89] Yariv, Amnon. *Quantum Electronics.* New York : John Wiley & Sons, 1989.

Appendix

The following files are Mathematica files used in generating several of the tables and figures included in this report. Section A contains the file used to generated the nonlinear parameters tabulated in Chapter 3. Section B has sample files for calculating conversion efficiencies for both the critically and noncritically phase matched crystals, using the jacobian equation as discussed in Chapter 4. Section C of the appendix includes the heat flow formulas detailed in section 7.2.

A Calculating Nonlinear Parameters

```
(* Mathematica file for generating nonlinear optical parameters *)
(* All values for a 1 cm long BBO crystal with 100MW pk power*)

(* Constants *)

no1 := 1.65510          (* indices of refraction for ordinary no and  *)
ne1 := 1.54254          (* extraordinary ne axes.  The numeral refers *)
no2 := 1.65510          (* to the frequency w, where w1 <= w2 < w3.   *)
ne2 := 1.54254
no3 := 1.67493
ne3 := 1.55552

a := 1                  (* scaling factors *)
b := 1
c := 2


(* Phase matching angle  - theta *)

(* Type I *)

avn := 1/c (a no1 + b no2)
thetaI := ArcSin[Sqrt[ (1/avn^2 - 1/no3^2)/(1/ne3^2 - 1/no3^2)]]

(* Type II *)
(* This parameter must be calculated using :     *)
(* Solve[lhs == rhs, theta].                     *)

lhs[theta_] := 1/Sqrt[(Cos[theta]^2/(no3)^2) + (Sin[theta]^2/(ne3)^2)]

rhs[theta_] := 1/c ( b no2 +
                     a 1/Sqrt[Cos[theta]^2/(no1)^2 + Sin[theta]^2/(ne1)^2])
```

```
(* Type III *)
(* note:  lhs is the same for both type II and type III *)

rhsIII[theta_] := 1/c ( a no1 + b 1/Sqrt[Cos[theta]^2/(no2)^2 + Sin[theta]^2/(ne2)^

(* Angular sensitivity - beta *)

(* Type I *)
betaI[theta_] := N[2 Pi c/ (1.064 10^(-4)) Sin[theta] Cos[theta] (1/ne3^2 -
1/no3^2) / ( (Cos[theta]^2/no3^2) + (Sin[theta]^2/ne3^2))^1.5]

(* Type II *)
betaII[theta_] := N[2 Pi / (1.064 10^(-4)) Sin[theta] Cos[theta] (c (1/ne3^2 -
1/no3^2)/( (Cos[theta]^2/no3^2) + (Sin[theta]^2/ne3^2))^1.5 - a (1/ne1^2 -
1/no1^2)/( (Cos[theta]^2/no1^2) + (Sin[theta]^2/ne1^2))^1.5)]

(* Type III *)
betaIII[theta_] := N[2 Pi/ (1.064 10^(-4)) Sin[theta] Cos[theta]
(a (1/ne3^2 - 1/no3^2)/( (Cos[theta]^2/no3^2) + (Sin[theta]^2/ne3^2))^1.5
- b (1/ne2^2 - 1/no2^2)/( (Cos[theta]^2/no2^2) + (Sin[theta]^2/ne2^2))^1.5)]

(* Angular bandwidth (FWHM) - delta theta *)

delth[beta_] := 4 1.39156 / beta

(* d effective -  units of pm/Volt*)

deffI[theta_] := .080 Sin[theta] - 1.6 Cos[theta]

deffII[theta_] := 1.6 Cos[theta]^2

(* Threshold Power - use the appropriate ccX for the type of phase matching X*)
(* cc corresponds to the c parameter  with units GW^(-1/2) 1064 is          *)
(* the wavelenght in microns *)

ccI[deff_] := 5.456 deff / (1.064 Sqrt[no1 no2 ne3])
ccII[deff_] := 5.456 deff / (1.064 Sqrt[ne1 no2 ne3])
ccIII[deff_] := 5.456 deff / (1.064 Sqrt[no1 ne2 ne3])

power[cc_,beta_] := (beta 1.064 10^(-4) / cc)^2

(* Drive - for Intensity = 100 10^6 Watts/cm^2*)

drive[cc_] := cc^2 100 10^6
```

B Calculating Conversion Efficiencies

B.1 Critically Phase Matched Crystals

```
(* This routine calculates and plots the jacobian formulation for the
   conversion efficiency versus crystal length.                        *)

(* Constants *)

c := 2.66                  (* GW^(-1/2) *)
intensity := 0.18          (* GW/cm^2 *)
beta := 10900              (* angular sensitvity *)
                           (* 1/(cm-rad)  *)
lambda := 1.064 10^-4      (* cm *)
q := 1.0                   (* beam quality factor *)
ws := 0.6                  (* beam diameter *)
                           (* cm *)

(* Equations *)

dk := beta lambda q/ws           (* Phase mismatch *)
no[l_] := c^2 l^2 intensity      (* drive *)


(* Jacobian Efficiency Equation *)

eta3[l_]:= Tanh[0.5 ArcTanh[
                JacobiSN[2 Sqrt[no[l]],1 + (.5 dk l)^2/(4 no[l])]]]^2


(* Plotting Routine *)

jacobplot := Plot[eta3[l],{l,0,1},PlotRange->{0,.5},PlotLabel->
                "BBO Type I Doubling",AxesLabel->{"Length","%"}]
```

B.2 Noncritically Phase Matched Crystals

```
(* Mathematica file for generating the efficiency vs. length for  *)
(* the noncritically phase-matched LBO doubler.                    *)


(* Constants *)

c := 1.94                 (* GW^(-1/2)  *)
intensity := 0.2          (* GW         *)
betat := 14.6912          (* 1/(C-cm)   *)
deltat := .1              (* degrees C  *)
lambda :=  1.064 10^-4    (* cm         *)
q := 1.0                  (* quality factor *)
ws := 0.4                 (* diameter cm    *)


(* Equations *)

dk := betat deltat                (* phase mismatch *)
no[l_] := c^2 l^2 intensity       (* drive *)

(* Efficiency Calculation *)

eta[l_]:= Tanh[0.5 ArcTanh[JacobiSN[2 Sqrt[no[l]],1 + (.5 dk l)^2/(4 no[l])]]]^2


(* Plotting Command *)

jacobplot := Plot[eta[l],{l,0,5},PlotRange->{{0,2},{0,1}},PlotLabel->FontForm[
"LBO Type I NCPM Doubler","Bold",14],AxesLabel->{FontForm["Length","Bold",14],
FontForm["%", "Bold", 14]}]
```

C Calculating Heat Flow

```
(* Heat flow in cylinder and slab geometries*)

k := .08 (1/100)                    (* conductivity  [W/cm*K] *)
alpha := .32                        (* absorption coefficient *)
power := .25                        (* power  [W]             *)
t :=  .4                            (* thickness  [cm]        *)


(* Volumetric heat flow into cylinder - Carslaw pg. 191*)

tempV[r_,R_] := (power alpha)/(Pi R^2 4 k t) ( R^2-r^2)

tempVplot := Plot[tempV[x,R],{x,0,R}, PlotLabel->"Temp vs. Radius in a
Cylinder", AxesLabel->{"Radius", "Temperature"}]

trdelplot := Plot[tempV[0,R],{R,0,2}, PlotLabel->"Temperature @ center
vs. Radii", AxesLabel->{"cylinder radius","Center Temp"},PlotRange->{0,3}]


(* Volumetric heat flow in a slab -L < x < L - Carslaw pg. 130 steady state*)

tempX[x_,L_] := (power alpha)/(2 (2 L) t k) (L^2 - x^2)
tempt[thick_] := (power alpha)/(2 (2 L) thick k) (L^2)

txdelplot := Plot[tempX[0,L],{L,0,2},PlotLabel->"Temp at center vs Slab
Thickness", AxesLabel->{"Thickness","Temp at Center"}]

tempXplot := Plot[tempX[x,L],{x,-L,L}, PlotRange->All, PlotLabel->"Temp vs.
thickness in slab"]

slabthicplot := Plot[tempt[th],{th,0,10}]
```